Discovery and characterization of 2-Anilino-4-(Thiazol-5-yl)Pyrimidine transcriptional CDK inhibitors as anticancer agents

Version: Accepted Manuscript

Link(s) to article on publisher's website:
http://dx.doi.org/doi:10.1016/j.chembiol.2010.07.016

Discovery and Characterisation of 2-Anilino-4-(thiazol-5-yl)pyrimidine Transcriptional CDK Inhibitors as Anticancer Agents

Shudong Wang,[1,2] Gary Griffiths,[1] Carol A. Midgley,[1] Anna L. Barnett,[1] Michael Cooper,[1] Joanna Grabarek,[1] Laura Ingram,[1] Wayne Jackson,[1] George Kontopidis,[1,3] Steven J. McClue,[1] Campbell McInnes,[1,4] Janice McLachlan,[1] Christopher Meades,[1] Mokdad Mezna,[1] Iain Stuart,[1] Mark P. Thomas,[1] Daniella I. Zheleva,[1] David P. Lane,[1] Robert C. Jackson,[1] David M. Glover,[1] David G. Blake,[1,*] and Peter M. Fischer[1,2,*]

[1]Cyclacel Limited, Dundee DD1 5JJ, Scotland, UK
[2]Present address: School of Pharmacy and Centre for Biomolecular Sciences, University of Nottingham, Nottingham NG7 2RD, UK
[3]Present address: Veterinary School, University of Thessaly, Karditsa 43100, Greece
[4]Present address: South Carolina College of Pharmacy, University of South Carolina, Columbia, SC 29208, USA
*Correspondence: dblake@cyclacel.com (D.G.B), peter.fischer@nottingham.ac.uk (P.M.F)

Running Title: Transcriptional CDK inhibitors

SUMMARY

The main difficulty in the development of ATP antagonist kinase inhibitors is target specificity, since the ATP-binding motif is present in many proteins. We introduce a strategy that has allowed us to identify compounds from a kinase inhibitor library that block the cyclin-dependent kinases responsible for regulating transcription, *i.e.* CDK7 and especially CDK9. The screening cascade employs cellular phenotypic assays based on mitotic index and nuclear p53 protein accumulation. This permitted us to classify compounds into transcriptional, cell cycle, and mitotic inhibitor groups. We describe the characterisation of the transcriptional inhibitor class in terms of kinase inhibition profile, cellular mode of action, and selectivity for transformed cells. A structural selectivity rationale was used to optimise potency and biopharmaceutical properties and led to the development of a transcriptional inhibitor, 3,4-dimethyl-5-[2-(4-piperazin-1-yl-phenylamino)-pyrimidin-4-yl]-3*H*-thiazol-2-one, with anticancer activity in animal models.

Introduction

Cyclin-dependent kinases (CDKs) are key cell cycle regulators and some also have regulatory functions in mRNA transcription at the level of RNA polymerase-II (RNAP-II) (Hirose et al., 2007). CDKs 1, 2, 7, 8, 9, and 11 have all been implicated in the phosphorylation of the C-terminal domain (CTD) of the largest RNAP-II subunit (Pinhero et al., 2004), but the most important ones are CDK7–cyclin H and CDK9–cyclin T (Ramanathan et al., 2001). The CTD contains repeating Tyr-Ser-Pro-Thr-Ser-Pro-Ser heptad sequences and the phosphorylation status of the Ser residues at positions 2 and 5 has been shown to be important in the activation of RNAP-II.

CDK7–cyclin H associates with the RING-finger protein MAT1 in the general transcription factor IIH (TFIIH) and also acts as an activating kinase for other CDKs. Unlike other CDKs, CDK9 appears to function exclusively in transcriptional regulation. It forms complexes with cyclin T1, T2, or K, which participate in the positive transcription elongation factor b (P-TEFb) (Michels et al., 2003). CDK9 phosphorylates both Ser-2 and Ser-5 of the CTD heptad (Pinhero et al., 2004), playing a predominant role during transcriptional elongation, in contrast to CDK7, which primarily phosphorylates Ser-5 of RNAP-II at the promoter as part of transcriptional initiation (Gomes et al., 2006).

Overexpression of cyclins or suppression of CDK-inhibitory proteins (CDKIs) is frequently observed in cancers and ectopic expression of CDKIs in tumour cells restores cell cycle control, leading to cell cycle arrest or apoptosis (Shapiro et al., 1999). However, it is now clear that many CDKs and cyclins associated with the cell cycle are functionally redundant, which suggests that targeting individual cell cycle CDKs may not be an optimal therapeutic strategy (Barriere et al., 2007). The anticancer activity in preclinical models of the experimental CDK inhibitor drugs flavopiridol (alvocidib; Aventis/NCI) and *R*-roscovitine (seliciclib, CYC202; Cyclacel) are believed to result mostly from the transcriptional inhibition mechanism (Fischer et al., 2005). Flavopiridol targets a number of CDKs and other kinases, and transcription inhibition caused by this compound in cancer cells was originally thought to be mediated by inhibition of CDK7 (Harper et al., 1998). Recent data, however, suggest that CDK9 inhibition plays a more important role (Chen et al., 2005). Treatment of cancer cells with flavopiridol results in inhibition of RNAP-II CTD phosphorylation, thus blocking transcription and inducing apoptosis by reducing mRNA levels of antiapoptotic proteins (Gojo et al., 2002). Selective induction of apoptosis in transformed cells by downregulation of antiapoptotic proteins through transcriptional CDK inhibition has also been demonstrated for *R*-roscovitine (MacCallum et al., 2005).

Clinical trials results show flavopiridol monotherapy efficacy in haematological cancers, especially chronic lymphocytic leukaemia, which is particularly sensitive to transcriptional inhibition (Byrd et al., 2007). Many clinical and preclinical pan-CDK inhibitor compounds

are potent CDK9 inhibitors and their antiproliferative properties emanate from transcriptional inhibition to a large extent (Joshi et al., 2007; Karaman et al., 2008; Wang et al., 2008; Zhang et al., 2008). However, truly CDK7- and CDK9-selective compounds have not been reported to date (Wang et al., 2008).

Here we report the results that have led to the identification of potent and selective new pharmacological CDK transcriptional inhibitors from our 2-anilino-4-(heteroaryl)-pyrimidine kinase inhibitor compound library (Wang et al., 2004a; Wang et al., 2004b; Wu et al., 2003). We have developed a cell-based screening cascade that has enabled us effectively to delineate a pharmacophore subseries of compounds characterised by selective antiproliferative effects in tumour cells through transcriptional CDK inhibition. This cascade has permitted us to distinguish phenotypically and biochemically compounds that inhibit RNAP-II CDKs from those that act predominantly through inhibition of the cell cycle CDKs (1, 2, 4), or the closely related mitotic aurora kinases. We use assays for mitotic index (MI), and p53 protein level measurements as a proxy measure for general transcriptional inhibition, for initial mechanistic compound classification, followed by more specific cell biological screens, such as caspase-3/7 activation assays, for more detailed compound mode-of-action analysis and classification (Griffiths et al., 2004; Griffiths et al., 2008; Wang et al., 2005; Wang et al., 2004a).

Results

Cellular phenotypic classification

The effects of treatment of A2780 (ovarian), NCI-H460 (non-small cell lung), and A549 (lung) tumour cell lines with compounds from our kinase inhibitor library were assessed using high through-put cell biological assays based on an automated microscopy system. Amongst these, MI and p53 protein level assays were found to be the most informative for classification of the library subgroups that target the cell cycle or transcription, respectively. Based on time–course experiments, a 7-h treatment period with test compounds was chosen to identify maximum effects on cell cycle or induction of p53 protein levels. p53 expression is regulated at the level of protein stability, and the increase in p53 protein levels after treatment with transcriptional inhibitors, including flavopiridol, is attributed to the downregulation of Mdm2 (Demidenko et al., 2004; Lu et al., 2001; Radhakrishnan et al., 2006), which is a well-established negative regulator of p53 protein (Michael et al., 2003). Compounds were typically screened using a concentration range of 0.04–20 μM, which permitted assessment of both potency and phenotypic specificity. Examination of MI and p53 protein levels resulted in identification of three classes of compounds: class-1 compounds decreased MI and induced high levels of nuclear p53 protein;

class-2 compounds increased MI, but had minimal effects on p53 protein levels; and class-3 compounds decreased MI and had minimal effects on p53 levels. Representatives of each class of compounds were further evaluated by enzymatic screening and cellular mode-of-action investigations.

MI was used as an indicator of cell cycle status in unsynchronised proliferating cells. Figure 1a illustrates the response of A2780 cells and is representative across the concentration range (the results from a primary MI and p53 screen of a set of 220 compounds is shown in Figure S1). Class-2 compounds, exemplified by a compound we have designated MKI-1 (for mitotic kinase inhibitor), delayed cells in mitosis and increased the overall MI of the cell population. Many of these compounds were subsequently identified as selective inhibitors of aurora kinases (data not shown, (Wang et al., 2010)). Class-1 compounds such as **1**, **3**, **4**, **6**, **7**, and **14** (Table 1) decreased MI, indicating a reduction in the number of cycling cells (Figure 1a) and increased the number of cells with high levels of nuclear accumulation of p53, typically with a 3- to 6-fold increase in A2780 (Figure 1b). To determine if p53 induction was a result of a DNA damage response (Kastan et al., 1991), additional experiments were carried out using an independent DNA-damage response marker, phosphorylated histone H2AX (Rogakou et al., 1998). Treatment of MCF-7 cells with either doxorubicin, a classical DNA-damaging agent (Gewirtz, 1999), or **1** resulted in accumulation of p53 (Figure 1c). Treatment with **1** had no effect on the level of histone H2AX phosphorylation, which was increased substantially by doxorubicin (Figure S2). A likely mechanism of p53 accumulation for class-1 compounds is reduction in the transcription and expression of Mdm2, the ubiquitin ligase responsible for degradation of p53 (Lu et al., 2001). Direct evidence for this mechanism was obtained after detailed investigations with compound **14** (see below). Nuclear p53 protein levels were subsequently used as an indicator of general transcriptional inhibition and this correlated well with biochemical selectivity for CDK 7 and 9 inhibition (Figure 2).

The third class of inhibitors, exemplified by the compounds designated CCI-1 and CCI-2 (for cell cycle inhibitors) in Figure 1a & 1b, reduced MI but had no significant effect on p53 protein levels. These compounds were subsequently identified as selective cell cycle inhibitors, which cause stage-specific cell cycle arrest and prevent mitotic entry (Wang et al., 2005).

CDK transcriptional inhibitors induce apoptosis in tumour cells

Caspases 3 and 7 are the most crucial effector components of cell death pathways that culminate in the cleavage of a number of important cellular proteins (Fuentes-Prior et al., 2004). We found that all of the compounds that we had identified as transcriptional CDK inhibitors (class-1) were capable of inducing a caspase-3/7 response in tumour cell lines,

including A2780, NCI-H460, MES-SA (uterine sarcoma) and HT-29 (colon adenocarcinoma). When *e.g.* A2780 cells were treated with **1**, **3**, **4**, **6**, **7**, and **14** for 24 h, substantial induction of apoptosis was observed, typically a > 7-fold induction of caspase-3/7 activation, compared to class-2 (MKI-1 & 2) and class-3 compounds (CCI-1 & 2), or controls (Figure 1d). Caspase activation was only observed in transformed lines and not in the nontransformed foetal lung cell line WI-38, despite it being able to activate caspases 3/7 in response to other classes of compounds. In all cases full induction of caspase activity occurred over a narrow concentration range as an all-or-nothing response (Figure 3a). Selective induction of apoptosis in transformed lines was confirmed by TUNEL of A2780 and WI-38 cells treated with compound **14**. Cell cycle arrest was not detected, and TUNEL-positive cells originated from all stages of the cell cycle (Figure 3b). This was observed in all tumour cell lines tested where an intact caspase-3/7 pathway was present, irrespective of mutant or wild-type p53 status. Class-1 compounds thus lead to apoptotic tumour cell death, and not to a stage-specific cell cycle block.

CDK transcriptional inhibitor analogues: design and lead optimisation

The 2-anilinopyrimidine compounds in Table 1 were prepared using procedures as described (Wang et al., 2004a). Previously established SARs of a series of 2-anilino-4-(thiazol-5-yl)pyrimidines with respect to CDK2 suggested the importance of substituents at *C*2 of the thiazole ring (Wang et al., 2004a). Introduction of amino functions in the context of either *meta*- or *para*-substituted anilines at the pyrimidine *C*2 resulted in increased inhibition not only of CDK2, but also CDK9. CDK2-bound crystal structures of such compounds, *e.g.* **1**, reveal that the thiazole *C*2-amino group interacts strongly with the Asp^{145} and Lys^{33} side chains and enhances the hydrophobic interaction of the thiazol-4-yl methyl group with the Phe gatekeeper residue present in all CDKs (Phe^{80} in CDK2) (Wang et al., 2004a). In addition, a number of H-bonding interactions between the thiazole *C*2-alkylamino groups and Gln^{131} and Asp^{86} were also observed. Substitution of the thiazole *C*2 with bulkier groups such as phenyl, pyridyl, or other heterocycles, resulted in significantly reduced activity. The thiazol-4-yl methyl group was also found to be intolerant of modification. Certain *meta*- or *para*-substitutions of the aniline ring were well tolerated and manipulation of these substituents led to a number of inhibitors possessing varying CDK selectivity profiles. Similar substituents in the *ortho* position abolished CDK-inhibitory activity in all cases.

Application of our screening cascade revealed that compounds with the transcriptional inhibitor phenotype predominantly inhibit CDK7 and CDK9 and show varying selectivity towards other CDKs, in particular CDK2 and CDK4, in enzymatic assays (Figure 2). A derivative with a sulfonamide substituent at the aniline *meta* position and containing a methylamino group at the thiazole *C*2 position (**3**) was found to be one of the most potent

transcriptional inhibitors in the class (Table 1). This compound also showed considerable potency against CDK2–cyclin E and CDK4–cyclin D1. Furthermore, it exhibited potent *in vitro* antitumour activity in a number of cancer cell lines. Replacement of the methylamino with an ethylamino group at thiazole *C*2 afforded another comparatively selective inhibitor of CDK7 and CDK9 (**2**), although with reduced potency. This also resulted in a substantial reduction in antiproliferative activity against tumour cell lines.

Methylation of the sulfonamide at the *meta* position of the aniline ring (**4**) also reduced CDKs 9, 2, and 4 activity somewhat compared to compound **3**. Again this was accompanied by an antiproliferative potency reduction. Analogue **5**, which has a primary amino group at the thiazole *C*2 showed potency and selectivity profiles comparable to **4**. Similar antiproliferative activity was observed for both compounds. Replacement of the sulfonamide of **3** with a methylsulfonyl function afforded another picomolar CDK9 inhibitor (**6**) that retained similar potency and selectivity with respect to CDKs 1, 2, and compared to **3**. The structural modification resulted in 10-fold lower activity against CDK4, however. As expected, **6** also displayed potent cytotoxicity in cells. Keeping the aniline portion of **6** constant, but replacing the thiazole *C*2 substituent with the larger ethylamino group led to **7**, with 5-fold reduced inhibition of CDK2 and 3-fold reduced inhibition of CDK9 compared to **6**. An ethyl group on the sulfonamide function (**8**), rather than the methylsulfonamide in **5**, in the context of the thiazole *C*2 primary amine, resulted in slightly reduced potency throughout.

In order to assess if targeting CDK9 alone would be sufficient for a compound to exhibit the transcriptional inhibitor phenotype, a number of selective CDK9 inhibitors were designed. During lead optimisation we observed that introduction of bulky substituents at the *meta* position of the aniline resulted in unfavourable contacts with CDK1 and CDK2, whereas simple nonionisable alkyl functions at the *para* position were poorly tolerated in terms of CDK4 activity. Combination of such substitution patterns in individual compounds led to the 4-methyl-3-(morpholine-4-sulfonyl)aniline derivatives **9** and **10**. Both compounds were potent CDK9 inhibitors essentially devoid of activity against CDKs 1, 2, and 4, while retaining modest potency against CDK7. Application of **9** and **10** in the screening cascade revealed that both compounds clearly belonged to class-1. However, these compounds exhibited reduced cellular potency in comparison to other low nanomolar K_i CDK9 inhibitors, which, in contrast, were potent against one or more additional CDKs.

Structural modification by transposition of various sulfonamide or alkylsulfone functions from the *meta* to the *para* position of the aniline ring generally resulted in somewhat reduced potency against all CDKs except CDK2. Thus compound **11**, although active against CDK9, inhibits CDK2 with almost 100-fold higher potency. However, having

achieved optimal CDK9 selectivity over CDK2 and CDK4 with compounds such as **9** and **10**, we turned our attention to CDK7 inhibition. We discovered that a number of compounds with a 3*H*-thiazol-2-one (formula **II** in Table 1) rather than a thiazole (formula **I**) system at the pyrimidine *C*4 displayed enhanced potency against CDK7. This was especially true for analogues with a methylated thiazolone *N*3 and small electron-withdrawing aniline *meta* substituents, such as **12**. Addition of a methyl group at the aniline *para* position again improved selectivity and also afforded our most potent CDK7 inhibitor compound **13**.

As noted above, bulky aniline *para* substituents were not conducive to CDK9 selectivity. If, however, substituents containing an amino group that is charged at physiological pH were introduced at the *para* position in the context of the pyrimidinyl *C*4 thiazolone system, both CDK7 and CDK9 potency was preserved, while maintaining selectivity with respect to the other CDKs to some extent. The representative compound in this regard is **14**, which potently inhibits not only CDK7, but also CDK 9. CDKs 1, 2, 4, on the other hand, are inhibited at least 30-fold less potently.

Compound **14** was also assessed for its selectivity in a panel of closely related non-CDK kinases. The results in Table S1 show that a range of kinases are inhibited by **14** at the mid-nanomolar to low micromolar IC_{50} level. Considering the fact that **14** is a mid-picomolar IC_{50} CDK9 inhibitor and comparing with the non-CDK kinase inhibited most potently (VEGFR2 IC_{50} = 180 nM), this gives a selectivity of at least 400-fold. This compound was also passed through a more extensive protein kinase panel that contains kinases representing most signalling pathways. The results again show that certain non-CDK kinases are inhibited by **14**, but at concentrations several orders of magnitude higher than those relevant to CDK7 and CDK9 inhibition (Figure S3).

Compound **14** was further assessed for its biopharmaceutical properties (Table S2): it has low lipophilicity (logP = 1.1) and good aqueous solubility. Membrane permeability was moderate with a P_{app} value of 2.4×10^{-6} cm/s by Caco-2 monolayer assay. Furthermore, **14** exhibited good *in vitro* metabolic stability with a half-life of 50 min and low intrinsic clearance in a liver microsome assay. Plasma protein binding was also low (36% unbound fraction). In order to confirm this, **14** was subjected to rat pharmacokinetic (PK) analysis following a single intravenous (*iv*) dose of 5 mg/kg or an oral (*po*) dose of 50 mg/kg. Mean plasma concentrations were used to calculate the PK parameters (Table S2). The compound was found to be orally bioavailable (F = 70%) with a plasma half-life of ~ 5 h following *po* administration, and a large volume of distribution. The exposure values obtained show that multiples of *in vitro* bioactive concentrations can easily be achieved at good dose potency.

Structural rationale for potency and selectivity of transcriptional inhibitors

In order to determine the basis for the selectivity and potency of CDK7 and CDK9 inhibitors, we determined complex crystal structures with CDK2 for compounds **11** and **14** (Figure 4a–d). Furthermore, we used published X-ray crystal structures of CDK7 (Lolli et al., 2004) and CDK9 (Baumli et al., 2008).

The CDK7 and CDK9 selectivity of compound **14**, which contains a piperazine substituent at the aniline *para* position, can be rationalised by the replacement of Lys^{89} in CDK2 with smaller residues in CDK7 and CDK9 (Figure 4e & f). Our CDK2–**14** complex crystal structure reveals that the bulky piperazine ring results in unfavourable contacts with the Lys^{89} side chain (Figure 4d). As a result, this side chain is forced to change position from that observed in apo- and ATP-bound CDK2 structures (Brown et al., 1999; Wu et al., 2003), which is energetically unfavourable. On the other hand, modelling suggests that the residues corresponding to Lys^{89} in CDK2, *i.e.* Val^{100} in CDK7 or Gly^{112} in CDK9 can better accommodate the piperazine ring of **14**. The complex structure of compound **14** with CDK2 and homology modelling with other CDKs further indicate that electrostatic charge differences at the ATP-binding site of CDK1 and CDK2 with respect to CDKs 4, 7, and 9 play a significant role in the selectivity of this compound. Because CDKs 4, 7, and 9 all have a nonionisable side chain in the Lys^{89} position, there is less repulsion with the positive charge on the piperazine ring (McInnes et al., 2004).

For compound **11**, which, unlike the piperazine ring of compound **14**, has a flexible sulfonamide substituent, the situation is different. Here the *p*-anilino sulfonamide can be observed to make strong H-bonding interactions with the side-chain amino group of Lys^{89} in CDK2 (Figure 4c). Similar interactions are not possible with CDK7 and CDK9, where small lipophilic residues are present in place of Lys^{89}.

The selectivity of the methylsulfone compounds **6** and **7** derives from differences in the residues that correspond to Gln^{131} in CDK2. This is Ala^{153} in CDK9, which is capable of forming favourable van-der-Waals contacts with the sulfone methyl groups. The increasing CDK9 selectivity of compounds **4**, **5**, and **8**–**10**, on the other hand, can be explained by the increase in steric bulk of the extensions of the sulfonamides at the aniline *meta* position. As we have shown, compounds with small aniline *meta* substituents – *e.g.* the nitro derivative **1**, adopt CDK2 binding poses with two distinct aniline orientations (Wang et al., 2004a). Modelling shows that unfavourable intramolecular interactions of the sulfonamide extensions in compounds **4**, **5**, and **8**–**10** with the thiazole/thiazolone head groups force the aniline rings to project towards the position occupied by Lys^{89} in CDK2, resulting in unfavourable contacts. From the crystal structures of CDK7 and CDK9 it is apparent that the region around Lys^{88}-Lys^{89} (in the CDK2 context) is considerably more open in CDK7 – and especially in CDK9 – due to the presence of the smaller side chains

of the corresponding residues (Glu^{99}-Val^{100} and Ala^{111}-Gly^{112} in CDK7 and CDK9 respectively).

Cellular mode of action of compound 14

In vitro antiproliferative activity. On the basis of its *in vitro* kinase potency, selectivity, and pharmaceutical properties, a detailed study of the cellular mode of action of **14** was carried out. It was screened against a panel of human leukaemia and solid tumour cell lines (Table S3). A broad spectrum of *in vitro* antitumour activity was observed, with an average IC_{50} value of 0.3 μM. There was no selectivity towards cell line types based on p53, p21, p16, or pRb status. Selectivity towards transformed *versus* untransformed cell lines was observed: **14** was 20- and 40-fold less potent against foetal lung fibroblast lines WI-38 and IMR-90, respectively, compared to the tumour cell lines examined.

RNAP-II CTD phosphorylation and p53 induction. In accordance with the biochemical enzyme inhibition data showing **14** to be a potent inhibitor of CDK7 and CDK9, the phosphorylation of both Ser-2 and Ser-5 of the RNAP-II CTD was reduced significantly after 3 h in A2780, with WI-38 cells showing a similar response at 24 h (Figure 5). Protein levels of p53 were induced at early time points since p53 is regulated at the translational level, but p21 levels, normally upregulated by p53-dependent transcription, did not rise due to inhibition of transcription by **14**.

Reduction of antiapoptotic protein levels. At 3 h, Mcl-1 levels were reduced in A2780 cells. After 24 h, A2780 and WI-38 cells both showed a reduction in antiapoptotic proteins XIAP, Mcl-1, and survivin (Figure 5). A2780 cells showed a greater reduction in levels of survivin and XIAP than WI-38 cells. Both cell lines showed reductions in Mcl-1. It is interesting to note that A2780 cells possess much greater levels of Mcl-1 than WI-38 in untreated samples.

Selective induction of apoptosis in transformed cells. Apoptosis is induced in A2780 cells, as detected by caspase-3/7 assay, at concentrations of 0.31 μM **14** and above. WI-38 cells, however, were completely insensitive even at 10 μM **14** (Figure 3a), despite showing sensitivity to mechanistically unrelated kinase inhibitor compounds. This result confirms the selectivity for transformed cells seen in the MTT proliferation assay (Table S3). TUNEL analysis, in conjunction with DNA staining, showed that 50% of cells were TUNEL-positive after 24 h with 2 μM **14** (Figure 3b). These apoptotic cells were observed in all cell cycle compartments, suggesting that this class of inhibitor causes cell death at each stage of the cell cycle and does not lead to a stage-specific cell cycle block. A reduction in the levels of antiapoptotic proteins occurred in both transformed (A2780) and untransformed (WI-38) cell lines. However, PARP cleavage (Figure 5) only occurred in the

A2780 cell line, suggesting that antiapoptotic proteins may play a less important role in the untransformed cells than in the oncogenically transformed cells.

Selective CDK9–cyclin T inhibition also induces the transcriptional-type response in cells. Compounds **3**, **10**, and in particular, compound **9**, showed greater selectivity for CDK9 over CDK7. Figure 2 shows that at the concentrations of compounds needed to induce cellular cytotoxicity, the contribution of CDK7 inhibition is negligible. From the screening cascade these compounds belonged to class-1 and further analysis of key cellular proteins showed a significant reduction in RNAP-II CTD Ser-2 phosphorylation, a slightly weaker reduction in Ser-5 phosphorylation, an induction of p53, and a reduction in Mcl-1 levels after 3 h exposure in A2780 cells (Figure S4). These responses are consistent with that shown by **14**, an approximately equipotent CDK7 and CDK9 inhibitor. Like **14**, the CDK9-specific inhibitors **3**, **9**, and **10** induced apoptosis selectively in transformed cells (Table S4).

In vivo anti-tumour activity of compound 14

Compound **14** was evaluated for *in vivo* antitumour activity using a P388/0 murine leukaemia survival model (Marsh et al., 1985). When dosed twice daily for 10 d with **14**, animals experienced an increase in life span of 68, 45, and 36% at doses of 30, 20 and 13 mg/kg/dose, respectively ($P < 0.0001$; Figure S5). The treated animals suffered no weight loss compared to animals receiving vehicle only and the maximum tolerated dose (MTD) of **14** was not achieved in this experiment, indicating a good therapeutic margin.

Compound **14** also demonstrated antitumour activity in a murine xenograft solid tumour model using the human colorectal Colo-205 cell line. As a positive control 5-fluorouracil (5-FU), the chemotherapy drug most commonly used in the clinic for colorectal cancer, was included on an optimal *iv* dosing regimen at the MTD. The test compound **14** was administered by either the intraperitoneal (*ip*) or oral route (Figure S6). When given at 50 mg/kg *ip* every day for 8 days, **14** produced a specific tumour growth delay of 10.5 days ($P < 0.05$). Similarly, **14** was active and well tolerated when given by the same schedule at 100 mg/kg *po*, resulting in a tumour growth delay of 7 days ($P < 0.05$). On the last evaluable day the tumour *versus* control ratios (T/C) were below 40% at the top dose by both administration routes. By comparison, 5-FU was considerably less active at its MTD of 50 mg/kg, given every 4 days for 4 treatments, and only yielded a tumour growth delay of 1 day.

Discussion

The work presented here explores the biomedical rationale for the development of pharmacological inhibitors of transcription. This effect is achieved with kinase inhibitors that

target predominantly CDK9–cyclin T1 and is further explored by studying the effects of simultaneously inhibiting CDK7 and CDK2, additional CDKs thought to be responsible for the regulation of RNAP-II activity through phosphorylation of its CTD.

The current model of RNAP-II regulation postulates a sequence in which CDK7 first phosphorylates CTD Ser-5 residues as part of transcription initiation (Sims et al., 2004). Subsequent dephosphorylation of Ser-2, and then phosphorylation of Ser-2 residues by CDK9 (Zhou et al., 2000) is necessary for the transition to RNA elongation (Price, 2000). Detailed analysis of CTD phosphorylation by CDKs 7, 8 and 9 (Ramanathan et al., 2001) have shown all three kinases to be capable of phosphorylating Ser-5, but not Ser-2, of a CTD peptide *in vitro*, despite evidence of *in vivo* phosphorylation at both Ser-2 and Ser-5 residues. This seems to correlate with the concept of stepwise phosphorylation, with Ser-5 phosphorylation being the initiating event, while Ser-2 becomes phosphorylated only after other criteria are met. Another study has highlighted the nonuniformity of CTD phosphorylation, showing that each of the three kinases produces different patterns of phosphorylation of the CTD, but that only CDK7 efficiently produces hyperphosphorylated substrates (Pinhero et al., 2004). These studies suggest that CTD phosphorylation is regulated in a complex manner, with changes in substrate specificity depending upon the transcriptional state of the complex and the accessibility of different regions of the CTD.

Each of our transcriptional-type inhibitor compounds is capable of reducing the phosphorylation of Ser-2 and Ser-5 of the CTD of RNAP-II. There is a differential response in the phosphorylation state of Ser-2 and Ser-5, with quicker and more pronounced dephosphorylation of Ser-2 over Ser-5. At this stage we cannot conclusively demonstrate kinase specificity for each site as this difference may be due to different phosphatase activities or site accessibility. However, compounds **3**, **9** and **10**, that we postulate to possess no appreciable CDK7 activity at the concentrations used to elicit a cytotoxic IC_{50} response (Figure 2), can still cause a reduction in Ser-2 phosphorylation after 3 h and initiate events that lead to the subsequent induction of apoptosis. This data lends support to the hypothesis of CDK9 targeting the Ser-2 site of RNAP-II and that inhibition of CDK9 is sufficient to inhibit transcription.

The transcriptional activity of RNAP-II is required in all cells and inhibition of RNAP-II may thus not immediately present itself as a rational target for cancer therapeutics. However, transformed cells have a greater requirement for enhanced transcriptional activity. Firstly, their increased rate of proliferation necessitates increased protein production. Secondly, cells are genetically predisposed to enter into programmed cell death upon oncogenic stimulation, but a few may be able to transform into an apoptosis-resistant, rapidly proliferating state by a number of means. One way of avoiding apoptotic death is the increased production of antiapoptotic proteins in order to counteract the

presence of the proapoptotic proteins induced by the initial transforming event (Koumenis et al., 1997). The cancer cell achieves a new balance, but at the expense of continuously increased production of these antiapoptotic proteins, many of which have short half-lives at both the mRNA and protein levels. The fully transformed cell is thus committed to a strategy of increased protein production and therefore increased transcription in order to maintain the *status quo* of cell survival over programmed cell death.

The increased production of antiapoptotic proteins in transformed cells is well documented (Liston et al., 2003; Schimmer, 2004). For example, elevated levels of survivin, XIAP, cIAP1, and cIAP2 have been shown in human prostate cancers and in prostate tissues from transgenic mice expressing SV40 large T antigen (Krajewska et al., 2003). Survivin is highly expressed in many transformed cells but is rarely detected in normal adult tissues (Zangemeister-Wittke et al., 2004). Mcl-1 is a member of the anti-apoptotic Bcl-2 family (Cory et al., 2003) whose expression decreases when cells undergo apoptosis (Iglesias-Serret et al., 2003). Increased Mcl-1 protein levels have been reported in a number of tumour samples (Khoury et al., 2003; Song et al., 2005), and a difference in expression may be observed in the control lanes of A2780 and WI-38 (Figure 5).

We show that as a result of decreased transcription, the expression levels of a number of highly expressed, short half-life, antiapoptotic proteins such as Mcl-1, survivin, and XIAP decline rapidly in both transformed and untransformed cell lines. We demonstrate that although the primary events of dephosphorylation of RNAP-II, induction of p53, and downregulation of antiapoptotic proteins, is consistent across transformed and untransformed lines, the ultimate fate of the cell is governed by its reliance upon antiapoptotic proteins for continued survival. This results in a selective apoptotic response, demonstrated by strong induction of caspase-3/7 activity, PARP cleavage, and appearance of TUNEL-positive cells in transformed cell lines only.

The induction of p53, a protein whose expression is tightly regulated at the posttranslational level by its association with Mdm2, itself a short half-life protein that is affected by reduced transcriptional activity, may contribute to the apoptotic response. p53 may translocate to the mitochondria and induce apoptosis through its direct interaction with, and activation of proapoptotic proteins such as Bax (Arima et al., 2005). However, as we see no differential sensitivity between p53 wild-type and p53 mutant or null cells in our cytotoxicity assays and have demonstrated that the response is not part of a DNA damage response, we conclude that this effect is not integral to compound mode of action and we simply utilise this induction as part of our screening cascade. The increase in p53 levels is not accompanied by increased p21 levels, (a protein normally regulated by p53 activity), a response in keeping with transcriptional inhibition.

The work described here highlights our current understanding of transcriptional-type CDK inhibitors and demonstrates how this knowledge can be adapted to provide an efficient screening cascade for the identification of such compounds. We have profiled a number of compounds with the ability to reduce the phosphorylation of Ser-2 and Ser-5 of the CTD of RNAP-II through inhibition of CDK9–cyclin T and CDK7–cyclin H and selectively kill transformed cells as a result of this inhibition. Our work shows that although both transformed and untransformed cells show a similar reduction in antiapoptotic proteins due to inhibition of RNAP-II CTD phosphorylation, untransformed WI-38 lung fibroblasts do not undergo apoptosis, thus demonstrating a differential response to the downstream events that cause transformed cells to undergo apoptosis through the caspase pathway. *In vivo* experiments have also demonstrated a good tolerance for compound **14** and significant increases in life span and antitumour activity in mouse models. We thus conclude that an untransformed cell, with intact checkpoints, low oncogenic stress, and lower levels of apoptotic proteins may have a significant tolerance towards transient inhibition of RNAP-II activity, whereas the equivalent transformed cell would be much more susceptible to this type of inhibition and undergo a caspase-induced apoptotic death.

Experimental procedures

Synthesis and compound characterisation

Preparation of *[4-(2-amino-4-methyl-thiazol-5-yl)-pyrimidin-2-yl]-(3-nitro-phenyl)-amine* (**1**) was described (Wang et al., 2004a). Compounds **2**–**10** were prepared in the same manner. Details are provided as Supplemental Experimental Procedures.

Cell-based assays

Mitotic index assay. MI was determined by an automated fluorescence microscopy 96-well plate assay using the Cellomics Arrayscan Mitotic Index HitKit protocol (Cellomics Inc.). Briefly, cells were plated at 10^4 cells per well and incubated for 18 h at 37 °C. Test compounds were added and cells were incubated for the appropriate time before a 15-min fixation in 3.7% formaldehyde in PBS. Cells were permeabilised in PBS with 0.2% triton X-100 for 15 min, washed, and incubated with a primary antibody that specifically recognises a mitotic epitope (rabbit anti-phosphoserine-10 histone-H3, Upstate 06-570). After incubation with a secondary FITC-conjugated anti-rabbit antibody and Hoechst 33258 dye, cells were washed and analysed using the Cellomics Arrayscan II automated fluorescent microscopy system to detect nuclear fluorescent staining. Data for 2,000 cells per well were collected and the Cellomics mitotic index algorithm used to calculate mitotic index (MI; percentage of cell nuclei stained with the mitosis-specific antibody *versus* total cell nuclei stained with Hoechst 33258 dye). A similar assay was carried out for DNA

damage by substituting a mouse antibody specific for the DNA damage marker histone H2AX (Upstate 17-327A) as the primary antibody and FITC-conjugated anti-mouse antibody as secondary antibody.

p53 Stabilisation assay. Cells were plated at 10^4 cells per well and incubated for 18 h at 37 °C. Test compounds were added and cells were incubated for the appropriate time before a 3-min fixation in cold (-20 °C) 50:50 v/v methanol/acetone. The fixed cells were dried briefly then washed with PBST (PBS, 0.1% triton X-100) and incubated with primary CM-1 rabbit anti-human p53 antiserum (Midgley et al., 1992) diluted 1:1,000. After incubation with a secondary Alexa Fluor 488 goat anti-rabbit antibody (Molecular Probes, A11008) and Hoechst dye, the cells were washed and analysed using the Cellomics Arrayscan II automated fluorescent microscopy system to detect nuclear fluorescent staining. Data for 2,000 cells per well were collected and the Cellomics mitotic index algorithm used to calculate percentage of cell nuclei stained with p53-specific antibody *versus* total cell nuclei stained with Hoechst.

MTT cytotoxicity assays. Standard MTT (thiazolyl blue; 3-[4,5-dimethylthiazol-2-yl]-2,5-diphenyltetrazolium bromide) assays were performed after 72 h treatment with test compounds (Haselsberger et al., 1996).

Determination of apoptosis. Apoptosis was determined by either a terminal deoxynucleotidyl transferase-mediated nick end labelling (TUNEL) assay (ApoDirect BD), following manufacturer's instructions, or by caspase-3/7 assay (Caspase-Glo 3/7 assay, Promega), following manufacturer's instructions, with cells seeded at 10,000 per well of a 96-well plate in a total volume of 100 µL medium per well. Assays were performed 24 h after test compound addition. Detection reagent (100 µL) was added directly to each 100-µL sample and readings were taken after a further 30 min incubation at room temperature.

Western blot analysis. Total protein cell lysates (10 µg) were run on SDS-PAGE (4-12% gradient) gels (Novex) under reducing conditions. The separated proteins were transferred to membranes and were probed with antibodies specific for pRb (BD), 249/252 pRb (BioSource), RNAP-II, RNAP-II Ser-2, RNAP-II Ser-5 (Covance), p53 (Oncogene ab-6), p21, PARP, Mcl-1 (Santa Cruz), XIAP, survivin (Novus), and actin (Sigma).

In vitro **kinase assays**

Details for the cloning, expression, and purification of His-tagged CDK9/Cyclin T1 are provided as Supplemental Experimental Procedures.

Kinase assays. CDK and other kinase assays were carried out as previously described (Wang et al., 2004a). IC_{50} values were calculated from 10-point dose-response curves

and apparent inhibition constants (K_i) were calculated from the IC_{50} values and appropriate K_m (ATP) values for the kinases in question (Cheng et al., 1973).

Pharmacology

Screening, biopharmaceutical profiling, PK determinations, and evaluation of anti-tumour efficacy of test compounds are described in the Supplemental Experimental Procedures.

Table 1. Structures and biological activity of selected CDK inhibitors.

No.	Structure			
	Formula	**R^1**	**R^2**	**R^3**
1	I	NH_2	NO_2	H
2	I	NHEt	SO_2NH_2	H
3	I	NHMe	SO_2NH_2	H
4	I	NHMe	SO_2NHMe	H
5	I	NH_2	SO_2NHMe	H
6	I	NHMe	SO_2Me	H
7	I	NHEt	SO_2Me	H
8	I	NH_2	SO_2NHEt	H
9	I	NHMe	SO_2-morpholine	Me
10	I	NH_2	SO_2-morpholine	Me
11	II	Me	H	$SO_2NH(CH_2)_2OMe$
12	II	Me	CN	H
13	II	Me	NO_2	Me
14	II	Me	H	Piperazine

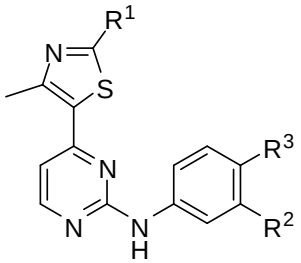

I

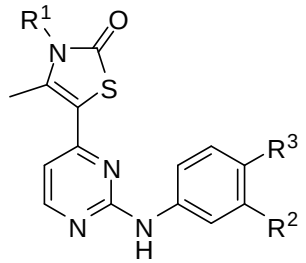

II

No.	Kinase inhibition, K_i (nM)					72-h MTT, IC_{50} (nM)	
	CDK1	*CDK2*	*CDK4*	*CDK7*	*CDK9*	*A2780*	*MES-SA*
1	73 ± 31	< 1	19 ± 17	73 ± 5	4.6 ± 5.2	41 ± 2	140 ± 13
2	691 ± 81	403 ± 29	132 ± 53	56 ± 24	4.5 ± 1.4	666 ± 106	1,608 ± 235
3	67 ± 11	2.4 ± 1.3	9.1 ± 2.9	25 ± 7	0.80 ± 0.79	12 ± 5	76 ± 10
4	334 ± 3	33 ± 1	20 ± 7	107 ± 71	4.3 ± 2.1	178 ± 44	278 ± 75
5	233 ± 32	26 ± 3	163 ± 73	127 ± 48	4.3 ± 1.8	205 ± 156	428 ± 45
6	86 ± 63	1.6 ± 0.2	94 ± 4	91 ± 13	0.29 ± 0.27	87 ± 2	93 ± 15
7	> 500	7.6 ± 1.5	139 ± 23	47 ± 24	0.96 ± 0.14	101 ± 2	50 ± 15
8	660 ± 353	47 ± 16	391 ± 50	193 ± 13	5.9 ± 1.5	332 ± 13	425 ± 65
9	> 500	> 500	> 500	3,469 ± 1,526	6.7 ± 3.0	760 ± 336	370 ± 43
10	> 500	> 500	> 500	304 ± 87	8.5 ± 1.3	692 ± 35	169 ± 45
11	4.1 ± 0.8	0.11 ± 0.05	> 500	940 ± 55	14 ± 2	221 ± 75	98 ± 10
12	399 ± 16	0.52 ± 0.11	102 ± 53	6.8 ± 3.0	1.9 ± 2.3	216 ± 20	367 ± 30
13	3.0 ± 0.5	28 ± 3	60 ± 18	0.56 ± 0.13	5.9 ± 3.3	34 ± 1	126 ± 30
14	449 ± 48	149 ± 40	68 ± 28	2.3 ± 0.2	0.38 ± 0.27	131 ± 9	150 ± 16

Figure 1. Identification of CDK transcriptional inhibitors by cell-based assays in A2780 cancer cells. Cells were treated with test compounds or assay diluent only (control) at 0.63 μM (**a**, **b**) or the concentrations indicated (**c**) for 7 h (**a**–**c**) or 24 h (**d**). MI was measured by determining the percentages of phospho-histone-H3 positive cells (**a**). Nuclear accumulation of p53 was assessed by immunofluorescent staining (**b**). Transcription inhibitors induce a time-dependent increase in p53 protein (**c**) and an apoptotic signal through activation of caspases-3/7 (**d**).

Figure 2. Cellular CDK selectivity. For each test compound the antiproliferative 72-h MTT assay IC_{50} value against A2780 cells was divided by the K_i values against individual CDKs (determined in biochemical kinase assays) and the ratios were plotted. A low ratio (ratios of ≤ 1 are shown as unity for the sake of clarity) indicates that antiproliferative activity is unlikely to be due to inhibition of the CDK in question. It is apparent that CDK9 inhibition is important for all transcriptional inhibitors (**1**–**10** & **14**). No other kinase tested shows such a correlation. Of the nontranscriptional inhibitors, **11**, **12**, and **CCI-2** show potentially significant cellular inhibition of CDK9 but these compounds also show strong activity against other kinases.

Figure 3. Selective induction of apoptosis in transformed cells. (**a**) Caspase-3/7 activation assays show **14** selectively to induce caspase activation in the transformed A2780 cell line but not in the nontransformed WI-38 line. Treatment with CCI-3 demonstrates caspase induction in both cell lines. (**b**) Flow cytometric analysis was performed and cell death (by TUNEL assay gating; ordinate) was correlated with cell cycle stage (by DNA content gating; abscissa). Cells were treated with assay diluent only (control) or with 2 μM compound **14** (treated) for 24 h. Treatment with **14** (2 μM) resulted in 31% TUNEL-positive A2780 cells corresponding to all cell cycle phases, whereas similar treatment of WI-38 cells gave rise to only 4.8% TUNEL-positive cells.

Figure 4. Structural basis for compound CDK selectivity. Electron density (grey mesh) and two plausible binding conformations (green and cyan CPK sticks) each for **14** (**a**) and **11** (**b**) (contoured at 1.2 and 1.0 σ, respectively) in the complex crystal structures with CDK2 (grey CPK surface). Observed interactions of **11** (**c**) and **14** (**d**) with the ATP-binding site of CDK2 (grey), corresponding residues from an aligned structure of a catalytically competent CDK2-cyclin A-ATP/Mg structure are shown (PDB # 1QMZ; salmon). Broken lines indicate energetically favourable (magenta) and unfavourable (black) interactions (distances are indicated in Å). Superimposition of the CDK2–**14** complex (grey) with a CDK9 (PDB # 3BLR; salmon; **e**) and a CDK7 crystal structure (PDB #

1UA2; salmon; **f**). The RMSD for the alignment of the CDK9 and CDK7 with the CDK2-**14** coordinates (all atoms / ATP-binding site) was 2.39 Å / 0.78 Å and 1.65 Å / 0.92 Å, respectively. For data collection and refinement statistics of the X-ray crystal structure complexes of CDK2 with compounds **11** and **14** refer to Table S5.

Figure 5. Status of key cellular proteins following treatment with compound 14. After exposure of A2780 cells to **14** (**a**) CTD phosphorylation of Ser-2 and Ser-5 of RNAP-II is significantly reduced after 3 h. p53 levels have increased and levels of the antiapoptotic protein Mcl-1 have been reduced, whilst XIAP remains fairly constant at early time points. There is no reduction in phosphorylation of pRb at the 249/252, 780 or 821 sites. After 24 h treatment with **14** (**b**) both the transformed A2780 and untransformed WI-38 cell lines show a similar primary response. There is a reduction in phosphorylation of the CTD of RNAP-II at Ser-2 and Ser-5, an increase in p53, and a decrease in each of the antiapoptotic proteins XIAP, Mcl-1, and survivin. Only A2780 cells show cleavage of PARP, however, suggesting that apoptosis has been initiated in these cells.

References

Arima, Y., Nitta, M., Kuninaka, S., Zhang, D., Fujiwara, T., Taya, Y., Nakao, M., and Saya, H. (2005). Transcriptional Blockade Induces p53-dependent Apoptosis Associated with Translocation of p53 to Mitochondria. J. Biol. Chem. *280*, 19166-19176.

Barriere, C., Santamaria, D., Cerqueira, A., Galan, J., Martin, A., Ortega, S., Malumbres, M., Dubus, P., and Barbacid, M. (2007). Mice thrive without Cdk4 and Cdk2. Mol. Oncol. *1*, 72-83.

Baumli, S., Lolli, G., Lowe, E.D., Troiani, S., Rusconi, L., Bullock, A.N., Debreczeni, J.E., Knapp, S., and Johnson, L.N. (2008). The structure of P-TEFb (CDK9/cyclin T1), its complex with flavopiridol and regulation by phosphorylation. EMBO J. *27*, 1907-1918.

Brown, N.R., Noble, M.E., Endicott, J.A., and Johnson, L.N. (1999). The structural basis for specificity of substrate and recruitment peptides for cyclin-dependent kinases. Nat. Cell Biol. *1*, 438-443.

Byrd, J.C., Lin, T.S., Dalton, J.T., Wu, D., Phelps, M.A., Fischer, B., Moran, M., Blum, K.A., Rovin, B., Brooker-McEldowney, M., Broering, S., Schaaf, L.J., Johnson, A.J., Lucas, D.M., Heerema, N.A., Lozanski, G., Young, D.C., Suarez, J.R., Colevas, A.D., and Grever, M.R. (2007). Flavopiridol administered using a pharmacologically derived schedule is associated with marked clinical efficacy in refractory, genetically high-risk chronic lymphocytic leukemia. Blood *109*, 399-404.

Chen, R., Keating, M.J., Gandhi, V., and Plunkett, W. (2005). Transcription inhibition by flavopiridol: mechanism of chronic lymphocytic leukemia cell death. Blood *106*, 2513-2519.

Cheng, Y.-C., and Prusoff, W.H. (1973). Relation between the inhibition constant IK1) and the concentration of inhibitor which causes fifty per cent inhibition (I50) of an enzymic reaction. Biochem. Pharmacol. *22*, 3099-3108.

Cory, S., Huang, D.C.S., and Adams, J.M. (2003). The Bcl-2 family: roles in cell survival and oncogenesis. Oncogene *22*, 8590-8607.

Demidenko, Z.N., and Blagosklonny, M.V. (2004). Flavopiridol induces p53 via initial inhibition of Mdm2 and p21 and, independently of p53, sensitizes apoptosis-reluctant cells to tumor necrosis factor. Cancer Res. *64*, 3653-3660.

Fischer, P.M., and Gianella-Borradori, A. (2005). Recent progress in the discovery and development of CDK inhibitors. Expert Opin. Investig. Drugs *14*, 457-477.

Fuentes-Prior, P., and Salvesen, G.S. (2004). The protein structures that shape caspase activity, specificity, activation and inhibition. Biochem. J. *384*, 201-232.

Gewirtz, D.A. (1999). A critical evaluation of the mechanisms of action proposed for the antitumor effects of the anthracycline antibiotics Adriamycin and daunorubicin. Biochem. Pharmacol. *57*, 727-741.

Gojo, I., Zhang, B., and Fenton, R.G. (2002). The Cyclin-dependent Kinase Inhibitor Flavopiridol Induces Apoptosis in Multiple Myeloma Cells through Transcriptional Repression and Down-Regulation of Mcl-1. Clin. Cancer Res. *8*, 3527-3538.

Griffiths, G., Midgley, C., Grabarek, J., Cooper, M., Glover, D., Ingram, L., Jackson, W., Meades, C., Mezna, M., O'Boyle, J., Wood, G., Yuill, R., Lane, D.P., Jackson, R., Fischer,

P.M., and Wang, S. (2004). Identification and characterization of kinase inhibitors that inhibit CDK2, CDK7 and CDK 9 activities, induce p53 and result in reduced proliferation and induction of apoptosis of human tumor cells. Proc. Am. Assoc. Cancer Res. *45*, Abs. 837.

Griffiths, G., Scaerou, F., Midgley, C., McClue, S., Tosh, C., Jackson, W., MacCallum, D., Wang, S., Fischer, P., Glover, D., and Zheleva, D. (2008). Anti-tumor activity of CYC116, a novel small molecule inhibitor of Aurora kinases and VEGFR2. Proc. Am. Assoc. Cancer Res. *49*, Abs. 5644.

Harper, J.W., and Elledge, S.J. (1998). The role of Cdk7 in CAK function, a retro-retrospective. Genes Dev. *12*, 285-289.

Haselsberger, K., Peterson, D.C., Thomas, D.G., and Darling, J.L. (1996). Assay of anticancer drugs in tissue culture: comparison of a tetrazolium-based assay and a protein binding dye assay in short-term cultures derived from human malignant glioma. Anti Cancer Drugs *7*, 331-338.

Hirose, Y., and Ohkuma, Y. (2007). Phosphorylation of the C-terminal domain of RNA polymerase II plays central roles in the integrated events of eucaryotic gene expression. J. Biochem. *141*, 601-608.

Iglesias-Serret, D., Pique, M., Gil, J., Pons, G., and Lopez, J.M. (2003). Transcriptional and translational control of Mcl-1 during apoptosis. Arch. Biochem. Biophys. *417*, 141-152.

Joshi, K.S., Rathos, M.J., Joshi, R.D., Sivakumar, M., Mascarenhas, M., Kamble, S., Lal, B., and Sharma, S. (2007). In vitro antitumor properties of a novel cyclin-dependent kinase inhibitor, P276-00. Mol. Cancer Ther. *6*, 918-925.

Karaman, M.W., Herrgard, S., Treiber, D.K., Gallant, P., Atteridge, C.E., Campbell, B.T., Chan, K.W., Ciceri, P., Davis, M.I., Edeen, P.T., Faraoni, R., Floyd, M., Hunt, J.P., Lockhart, D.J., Milanov, Z.V., Morrison, M.J., Pallares, G., Patel, H.K., Pritchard, S., Wodicka, L.M., and Zarrinkar, P.P. (2008). A quantitative analysis of kinase inhibitor selectivity. Nat. Biotechnol. *26*, 127-132.

Kastan, M.B., Onyekwere, O., Sidransky, D., Vogelstein, B., and Craig, R.W. (1991). Participation of p53 protein in the cellular response to DNA damage. Cancer Res. *51*, 6304-6311.

Khoury, J.D., Medeiros, L.J., Rassidakis, G.Z., McDonnell, T.J., Abruzzo, L.V., and Lai, R. (2003). Expression of Mcl-1 in mantle cell lymphoma is associated with high-grade morphology, a high proliferative state, and p53 overexpression. J. Pathol. *199*, 90-97.

Koumenis, C., and Giaccia, A. (1997). Transformed cells require continuous activity of RNA polymerase II to resist oncogene-induced apoptosis. Mol. Cell. Biol. *17*, 7306-7316.

Krajewska, M., Krajewski, S., Banares, S., Huang, X., Turner, B., Bubendorf, L., Kallioniemi Olli, P., Shabaik, A., Vitiello, A., Peehl, D., Gao, G.-J., and Reed John, C. (2003). Elevated expression of inhibitor of apoptosis proteins in prostate cancer. Clin. Cancer Res. *9*, 4914-4925.

Liston, P., Fong, W.G., and Korneluk, R.G. (2003). The inhibitors of apoptosis: there is more to life than Bcl2. Oncogene *22*, 8568-8580.

Lolli, G., Lowe, E.D., Brown, N.R., and Johnson, L.N. (2004). The Crystal Structure of Human CDK7 and Its Protein Recognition Properties. Structure *12*, 2067-2079.

Lu, W., Chen, L., Peng, Y., and Chen, J. (2001). Activation of p53 by roscovitine-mediated suppression of MDM2 expression. Oncogene *20*, 3206-3216.

MacCallum, D.E., Melville, J., Frame, S., Watt, K., Anderson, S., Gianella-Borradori, A., Lane, D.P., and Green, S.R. (2005). Seliciclib (CYC202, R-roscovitine) induces cell death in multiple myeloma cells by inhibition of RNA polymerase II-dependent transcription and down-regulation of Mcl-1. Cancer Res. *65*, 5399-5407.

Marsh, J.C., Shoemaker, R.H., and Suffness, M. (1985). Stability of the in vivo P388 leukemia model in evaluation of antitumor activity of natural products. Cancer Treat. Rep. *69*, 683-685.

McInnes, C., Wang, S., Anderson, S., O'Boyle, J., Jackson, W., Kontopidis, G., Meades, C., Mezna, M., Thomas, M., Wood, G., Lane, D.P., and Fischer, P.M. (2004). Structural determinants of CDK4 inhibition and design of selective ATP competitive inhibitors. Chem. Biol. *11*, 525-534.

Michael, D., and Oren, M. (2003). The p53-Mdm2 module and the ubiquitin system. Semin. Cancer Biol. *13*, 49-58.

Michels, A.A., Nguyen, V.T., Fraldi, A., Labas, V., Edwards, M., Bonnet, F., Lania, L., and Bensaude, O. (2003). MAQ1 and 7SK RNA interact with CDK9/cyclin T complexes in a transcription-dependent manner. Mol. Cell. Biol. *23*, 4859-4869.

Midgley, C.A., Fisher, C.J., Bartek, J., Vojtesek, B., Lane, D., and Barnes, D.M. (1992). Analysis of p53 expression in human tumors: an antibody raised against human p53 expressed in Escherichia coli. J. Cell Sci. *101*, 183-189.

Pinhero, R., Liaw, P., Bertens, K., and Yankulov, K. (2004). Three cyclin-dependent kinases preferentially phosphorylate different parts of the C-terminal domain of the large subunit of RNA polymerase II. Eur. J. Biochem. *271*, 1004-1014.

Price, D.H. (2000). P-TEFb, a cyclin-dependent kinase controlling elongation by RNA polymerase II. Mol. Cell. Biol. *20*, 2629-2634.

Radhakrishnan, S.K., and Gartel, A.L. (2006). A novel transcriptional inhibitor induces apoptosis in tumor cells and exhibits antiangiogenic activity. Cancer Res. *66*, 3264-3270.

Ramanathan, Y., Rajpara, S.M., Reza, S.M., Lees, E., Shuman, S., Mathews, M.B., and Pe'ery, T. (2001). Three RNA polymerase II carboxyl-terminal domain kinases display distinct substrate preferences. J. Biol. Chem. *276*, 10913-10920.

Rogakou, E.P., Pilch, D.R., Orr, A.H., Ivanova, V.S., and Bonner, W.M. (1998). DNA double-stranded breaks induce histone H2AX phosphorylation on serine 139. J. Biol. Chem. *273*, 5858-5868.

Schimmer, A.D. (2004). Inhibitor of Apoptosis Proteins: Translating Basic Knowledge into Clinical Practice. Cancer Res. *64*, 7183-7190.

Shapiro, G.I., and Harper, J.W. (1999). Anticancer drug targets: cell cycle and checkpoint control. J. Clin. Investig. *104*, 1645-1653.

Sims, R.J., Mandal, S.S., and Reinberg, D. (2004). Recent highlights of RNA-polymerase-II-mediated transcription. Curr. Opin. Cell Biol. *16*, 263-271.

Song, L., Coppola, D., Livingston, S., Cress, D., and Haura, E.B. (2005). Mcl-1 Regulates Survival and Sensitivity to Diverse Apoptotic Stimuli in Human Non-Small Cell Lung Cancer Cells. Cancer Biol. Ther. *4*, 267-276.

Wang, S., and Fischer, P.M. (2008). Cyclin-dependent kinase 9: a key transcriptional regulator and potential drug target in oncology, virology and cardiology. Trends Pharmacol. Sci. *29*, 302-313.

Wang, S., Griffiths, G., Midgley, C., Meades, C., O'Boyle, J., Gibson, D., Wood, G., Grabarek, J., Cooper, M., Mezna, M., Jackson, W., Perry, A., Stuart, I., McClue, S.J., McInnes, C., Thomas, M., Yuill, R., Westwood, R., Lane, D.P., Jackson, R.C., and Fischer, P.M. (2005). Discovery and evaluation of CDK transcriptional inhibitors as anti-cancer agents. Proc. Am. Assoc. Cancer Res. *46*, Abs. LB-110.

Wang, S., Meades, C., Wood, G., Osnowski, A., Anderson, S., Yuill, R., Thomas, M., Mezna, M., Jackson, W., Midgley, C., Griffiths, G., Fleming, I., Green, S., McNae, I., Wu, S.-Y., McInnes, C., Zheleva, D., Walkinshaw, M.D., and Fischer, P.M. (2004a). 2-Anilino-4-(thiazol-5-yl)pyrimidine CDK Inhibitors: Synthesis, SAR analysis, X-Ray Crystallography, and Biological Activity. J. Med. Chem. *47*, 1662-1675.

Wang, S., Midgley, C.A., Scaërou, F., Grabarek, J.B., Griffiths, G., Jackson, W., Kontopidis, G., McClue, S.J., McInnes, C., Meades, C., Mezna, M., Plater, A., Stuart, I., Thomas, M.P., Wood, G., Clarke, R.G., Blake, D.G., Zheleva, D.I., Lane, D.P., Jackson, R.C., Glover, D.M., and Fischer, P.M. (2010). Discovery of N-Phenyl-4-(thiazol-5-yl)pyrimidin-2-amine Aurora Kinase Inhibitors. J. Med. Chem. *53*, 4367-4378.

Wang, S., Wood, G., Meades, C., Griffiths, G., Midgley, C., McNae, I., McInnes, C., Anderson, S., Jackson, W., Mezna, M., Yuill, R., Walkinshaw, M., and Fischer, P.M. (2004b). Synthesis and Biological Activity of 2-Anilino-4-(1H-pyrrol-3-yl)pyrimidine CDK Inhibitors. Bioorg. Med. Chem. Lett. *14*, 4237-4240.

Wu, S.Y., McNae, I., Kontopidis, G., McClue, S.J., McInnes, C., Stewart, K.J., Wang, S., Zheleva, D.I., Marriage, H., Lane, D.P., Taylor, P., Fischer, P.M., and Walkinshaw, M.D. (2003). Discovery of a Novel Family of CDK Inhibitors with the Program LIDAEUS: Structural Basis for Ligand-Induced Disordering of the Activation Loop. Structure *11*, 399-410.

Zangemeister-Wittke, U., and Simon, H.-U. (2004). An IAP in action: the multiple roles of survivin in differentiation, immunity and malignancy. Cell Cycle *3*, 1121-1123.

Zhang, C., Lundgren, K., Yan, Z., Arango, M.E., Price, S., Huber, A., Higgins, J., Troche, G., Skaptason, J., Koudriakova, T., Nonomiya, J., Yang, M., O'Connor, P., Bender, S., Los, G., Lewis, C., and Jessen, B. (2008). Pharmacologic properties of AG-012986, a pan-cyclin-dependent kinase inhibitor with antitumor efficacy. Mol. Cancer Ther. *7*, 818-828.

Zhou, M., Halanski, M.A., Radonovich, M.F., Kashanchi, F., Peng, J., Price, D.H., and Brady, J.N. (2000). Tat modifies the activity of CDK9 to phosphorylate serine 5 of the RNA polymerase II carboxyl-terminal domain during human immunodeficiency virus type 1 transcription. Mol. Cell. Biol. *20*, 5077-5086.

Figure 1

Click here to download high resolution image

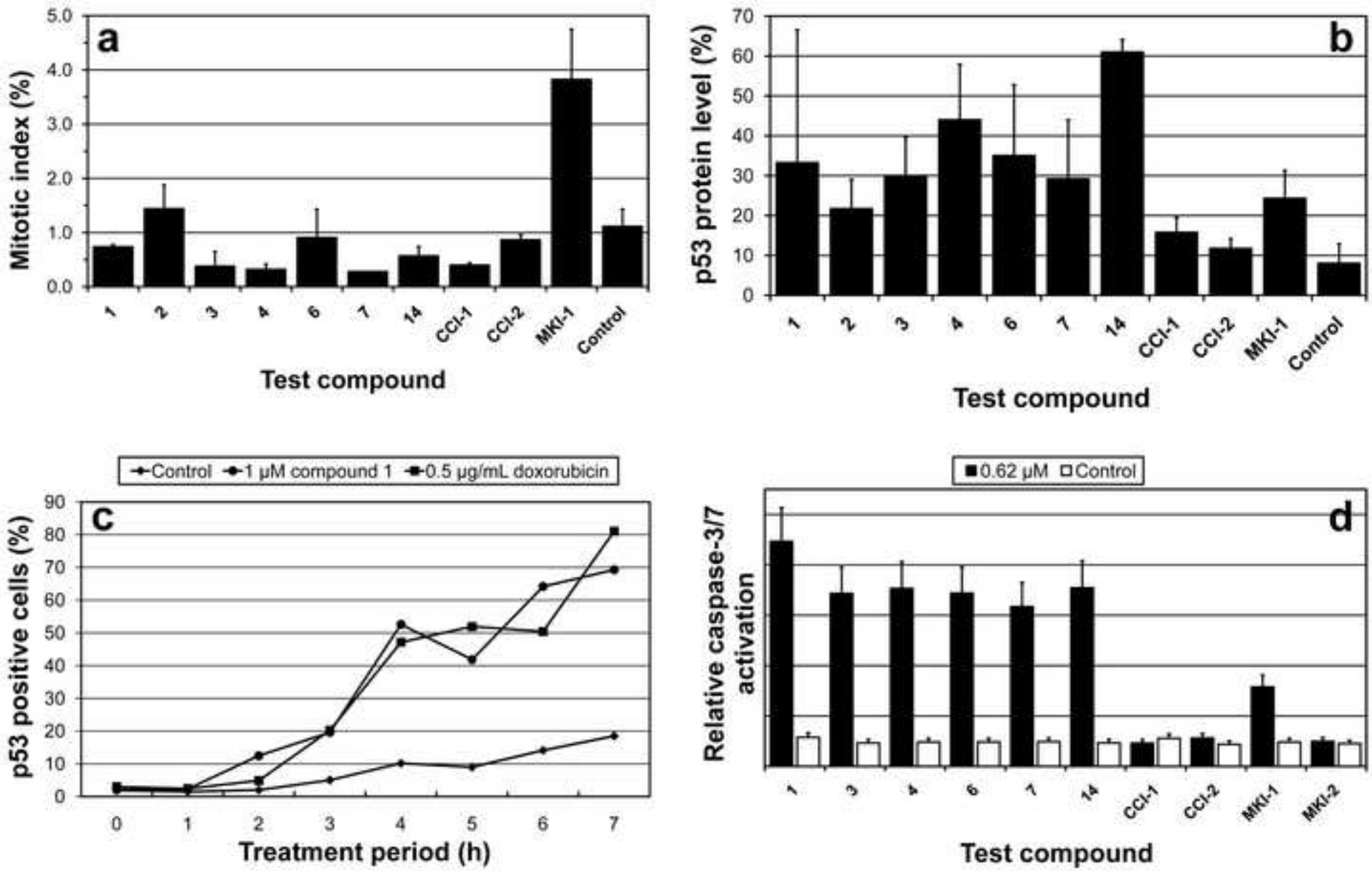

Figure 2

Click here to download high resolution image

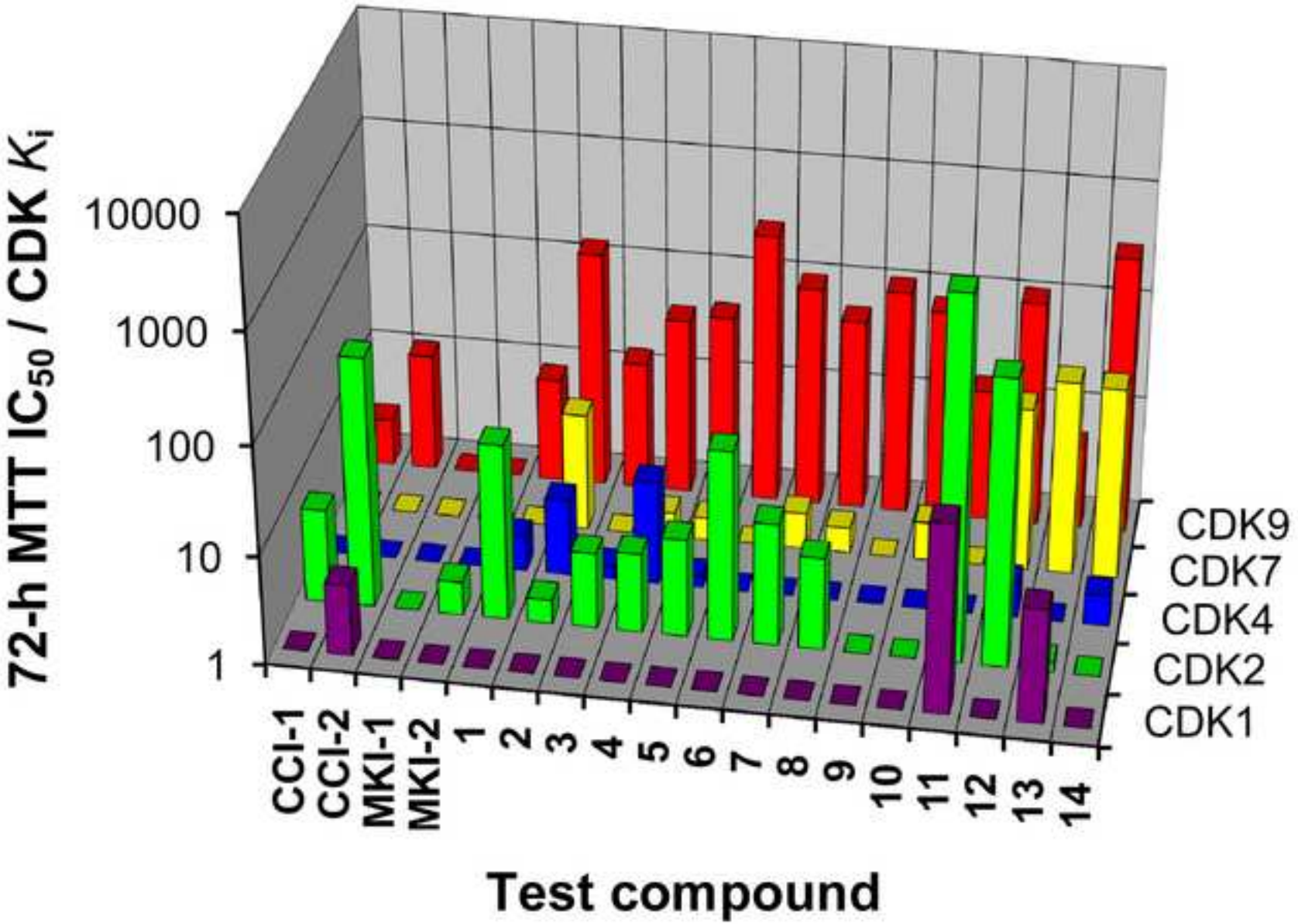

Figure 3

Click here to download high resolution image

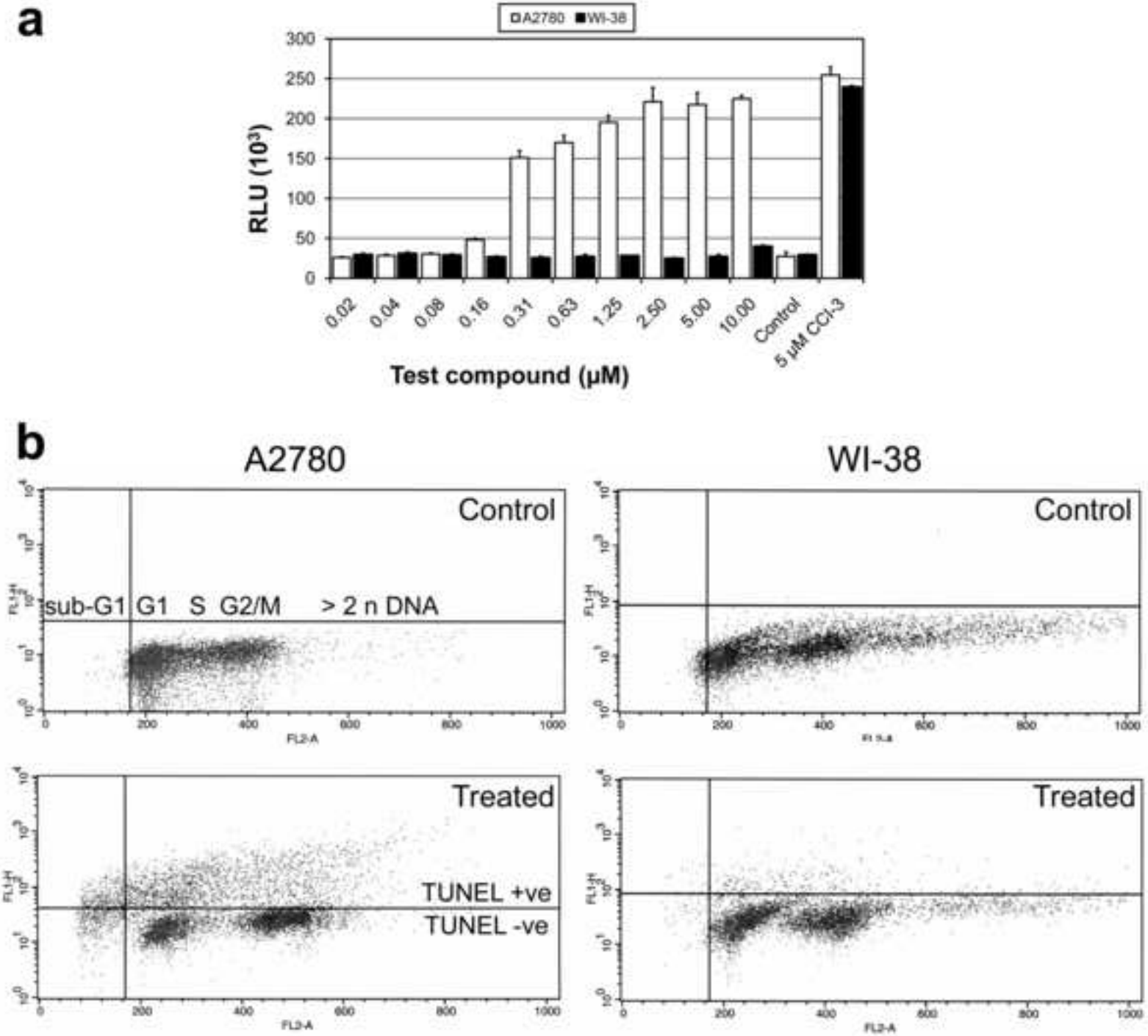

Figure 4

Click here to download high resolution image

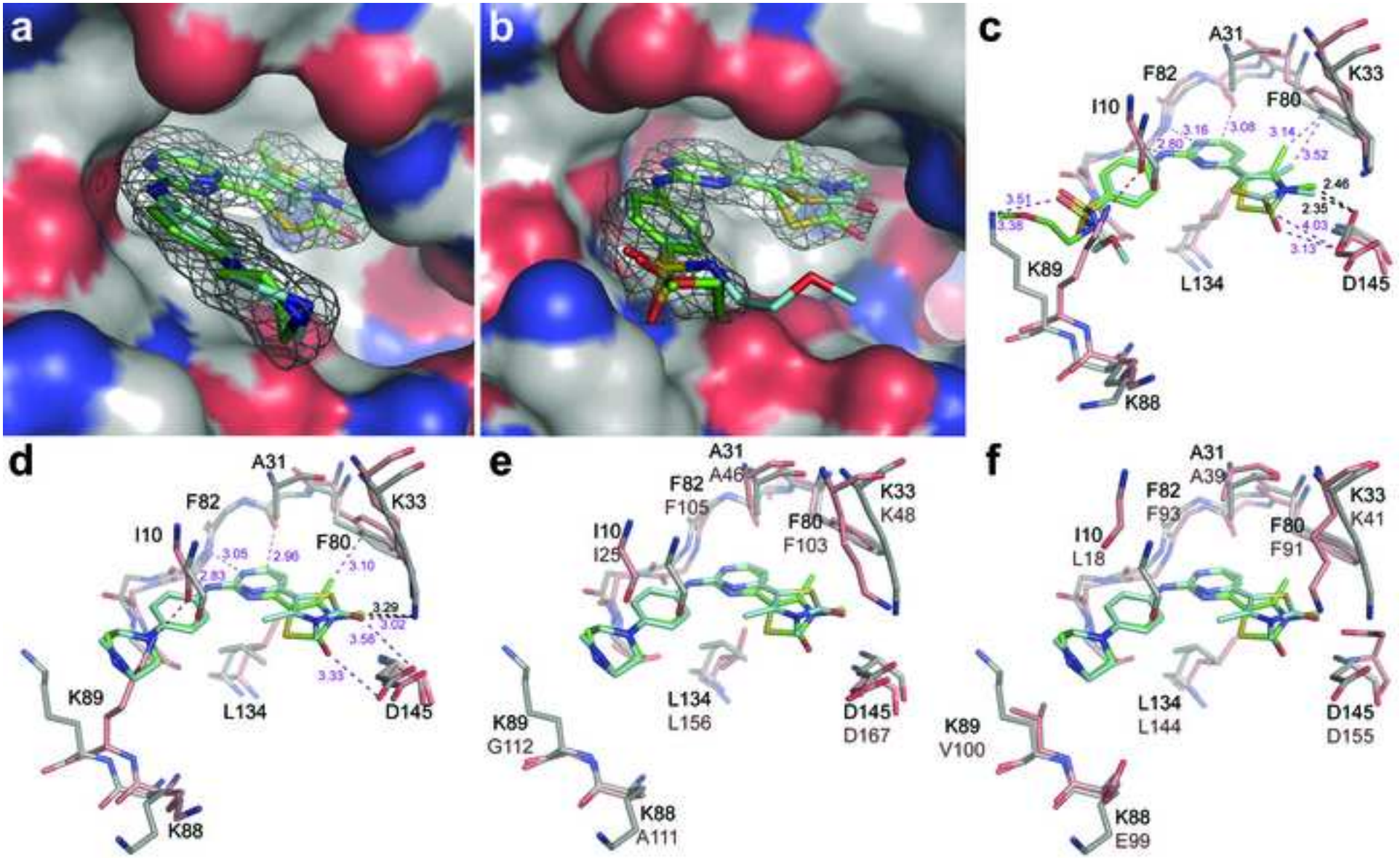

Figure 5

Click here to download high resolution image

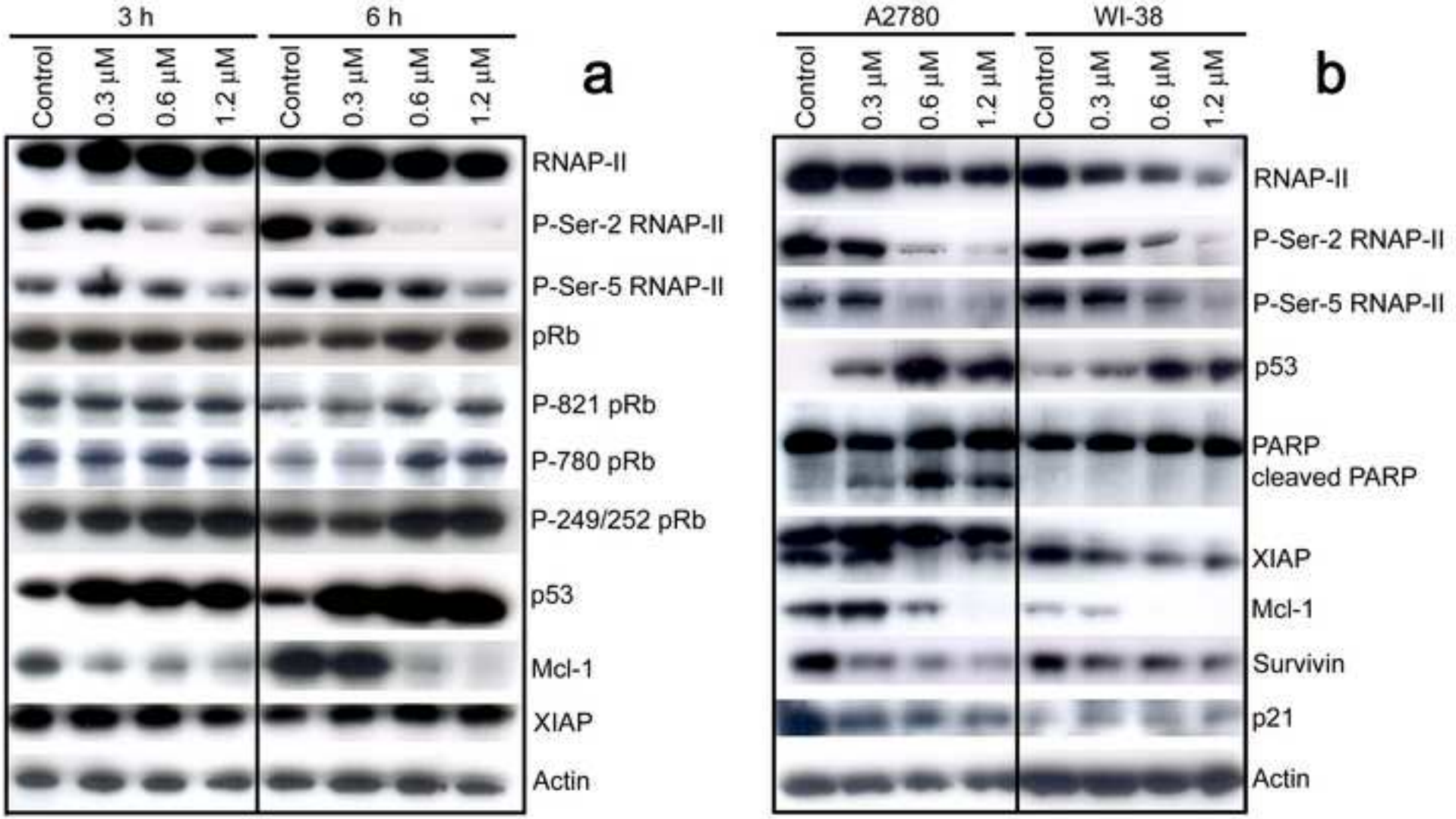

Supplemental information

Discovery and characterisation of 2-anilino-4-(thiazol-5-yl)pyrimidine transcriptional CDK inhibitors as anticancer agents

Shudong Wang,[1,2] Gary Griffiths,[1] Carol A. Midgley,[1] Anna L. Barnett,[1] Michael Cooper,[1] Joanna Grabarek,[1] Laura Ingram,[1] Wayne Jackson,[1] George Kontopidis,[1,3] Steven J. McClue,[1] Campbell McInnes,[1,4] Janice McLachlan,[1] Christopher Meades,[1] Mokdad Mezna,[1] Iain Stuart,[1] Mark P. Thomas,[1] Daniella I. Zheleva,[1] David P. Lane,[1] Robert C. Jackson,[1] David M. Glover,[1] David G. Blake,[1,*] and Peter M. Fischer[1,2,*]

[1]Cyclacel Limited, Dundee DD1 5JJ, Scotland, UK
[2]Present address: School of Pharmacy and Centre for Biomolecular Sciences, University of Nottingham, Nottingham NG7 2RD, UK
[3]Present address: Veterinary School, University of Thessaly, Karditsa 43100, Greece
[4]Present address: South Carolina College of Pharmacy, University of South Carolina, Columbia, SC 29208, USA
*Correspondence: dblake@cyclacel.com (D.G.B), peter.fischer@nottingham.ac.uk (P.M.F)

Table of contents

Table S2 (related to Table 1). *In vitro* kinase selectivity of compound **14**.

Kinase	**IC_{50} (μM)**[a]
Bcr-Abl	4.4 ± 0.2
Akt/PKB	> 10
CaMKII	> 10
CK2	> 10
ERK-2	> 10
GSK3b	0.39 ± 0.04
Lck	1.9 ± 0.1
PDGFb	0.80 ± 0.09
Plk1	> 10
PKA	> 10
PKC	> 10
S6	8.6 ± 3.7
SAPK2a	> 10
Src	2.0 ± 0.1
VEGFR2	0.18 ± 0.02
Aurora A	0.65 ± 0.06
Aurora B	0.40 ± 0.13

[a] Mean ± SD of at least two independent determinations; [ATP] = 0.1 mM.

Table S2 (related to Table 1). Biopharmaceutical and pharmacokinetic properties of compound **14**.

***In vitro* biopharmaceutical properties**			
Partition coefficient	$LogD_{7.4}$[a]	1.1	
Dissociation constants	pK_a[b]	8.3, 3.1	
Aqueous solubility[c]		> 100 μM	
Intestinal permeability	P_{app}[d] (10^{-6} cm/s)	2.4	
Microsomal stability[e]	CL_{int} (mL/min/mg)	27.5	
	$t_{1/2}$ (min)	50	
Plasma protein binding[f]	Fraction bound (%)	64	
Rat pharmacokinetics			
Pharmacokinetic parameter		5 mg/kg *iv*	50 mg/kg *po*
Exposure	$AUC_{0\text{-}24h}$ (h.μM)	1.5	10.4
Elimination	$t_{1/2}$ (h)	1.0	4.9
Clearance	CL (L/h/kg)	8.7	12.2
Volume of distribution	V_z-F (L/kg)	126	97
Oral bioavailability	(% F)		70

[a] Partitioning between octanol and aqueous buffer using the shake-flask method; [b] determined using a pH-metric method; [c] by turbidimetry; [d] apparent permeability coefficient measured using a Caco-2 cell layer assay; [e] measured by disappearance of parent compound (LC-MS) from a preparation of rat liver microsomes; [f] rat plasma protein binding using an equilibrium dialysis assay.

Table S3 (related to Table 1). Antiproliferative activity of compound **14**.

	Human cell line		72-h MTT
	Origin	*Designation*	IC_{50} ± SD (nM)
Transformed	Bone osteosarcoma	Saos-2	386 ± 189
		U2OS	372 ± 69
	Breast	MDA-MB-468	221 ± 56
		MCF-7	490 ± 358
	Cervix	Hela	401 ± 154
	Colon	HT29	280 ± 73
		LOVO	218 ± 118
		NCI-H1299	501 ± 207
		HCT-116	180 ± 44
	Gastric adenocarcinoma	AGS	256 ± 104
	Leukemia	CCRF-CEM	577 ± 438
	Promyelocytic leukaemia	HL60	374 ± 25
	Lung	A549	299 ± 93
		NCI-H460	264 ± 146
	Leiomyosarcoma	SKUT-1B	107 ± 43
		SKUT-1	225 ± 75
	Neuroblastoma	SK-N-MC	149 ± 24
	Ovarian carcinoma	A2780	131 ± 9
	Pancreatic carcinoma	Mia-Paca-2	139 ± 9
	Prostate	DU-145	140 ± 17
	Skin keratinocyte	Hacat	351 ± 122
	Uterine	Messa	150 ± 16
		Messa-Dx5	536 ± 260
Untransformed	Foetal lung fibroblast	IMR-90	12,278 ± 1,422
		WI38	5,748 ± 3,123
Mean transformed			293
Median transformed			264
Mean untransformed			9013

Table S4 (related to Figure 3). Selective induction of apoptosis in transformed cells by CDK9-selective compounds.

Treatment		**% Cells TUNEL-positive**[a]	
Test compound	Concentration (μM)	A2780 (Transformed)	WI-38 (Untransformed)
Compound **3**	0.2	8	NT
	1.0	63	3
Compound **9**	1.0	6	NT
	5.0	69	17
Compound **10**	1.0	2	NT
	5.0	53	10
Control		1	0

[a] TUNEL analysis of treated cells. A2780 or cycling WI-38 cells were treated with compounds for 24 h. Cells were analysed for DNA strand breaks by the TUNEL method. The percentages of cells labelled as TUNEL-positive are shown. All compounds show a greater selectivity for the transformed line over the untransformed one. NT-not tested.

Table S5 (related to Figure 4). Data collection and refinement statistics for X-ray crystal structure complexes of CDK2 with compounds **11** and **14**.

Data collection	CDK2-compound **11**	CDK2-compound **14**
Space group	$P2_12_12_1$	$P2_12_12_1$
Unit cell dimensions; a, b, c (Å)	53.12, 71.50, 71.64	53.00, 71.11, 72.03
Maximum resolution (Å)	1.9	1.8
Total observations	67,708	67,264
Unique reflections	21,623	25,565
Completeness (%)	97.9	98.8
R_{merge}	0.078	0.075
$<I / \sigma I>$	7.9	7.3
R_{merge}, highest resolution bin	0.415	0.485
$<I / \sigma I>$, highest resolution bin	2.3	2.1
Refinement		
Protein atoms	2,404	2,487
Ligand atoms	58	54
Water molecules	255	271
Reflections used in refinement	20,724	22,796
R_{work}	18.9	21.1
R_{free}	27.1	29.5
Mean B-factor, protein ($Å^2$)	52.1	48.8
Mean B-factor, ligands ($Å^2$)	57.8	40.2
Mean B-factor, solvent ($Å^2$)	58.5	53.4
Bond lengths from ideal values RMSD (Å)	0.011	0.012
Bond angles from ideal values RMSD (degrees)	1.69	1.60

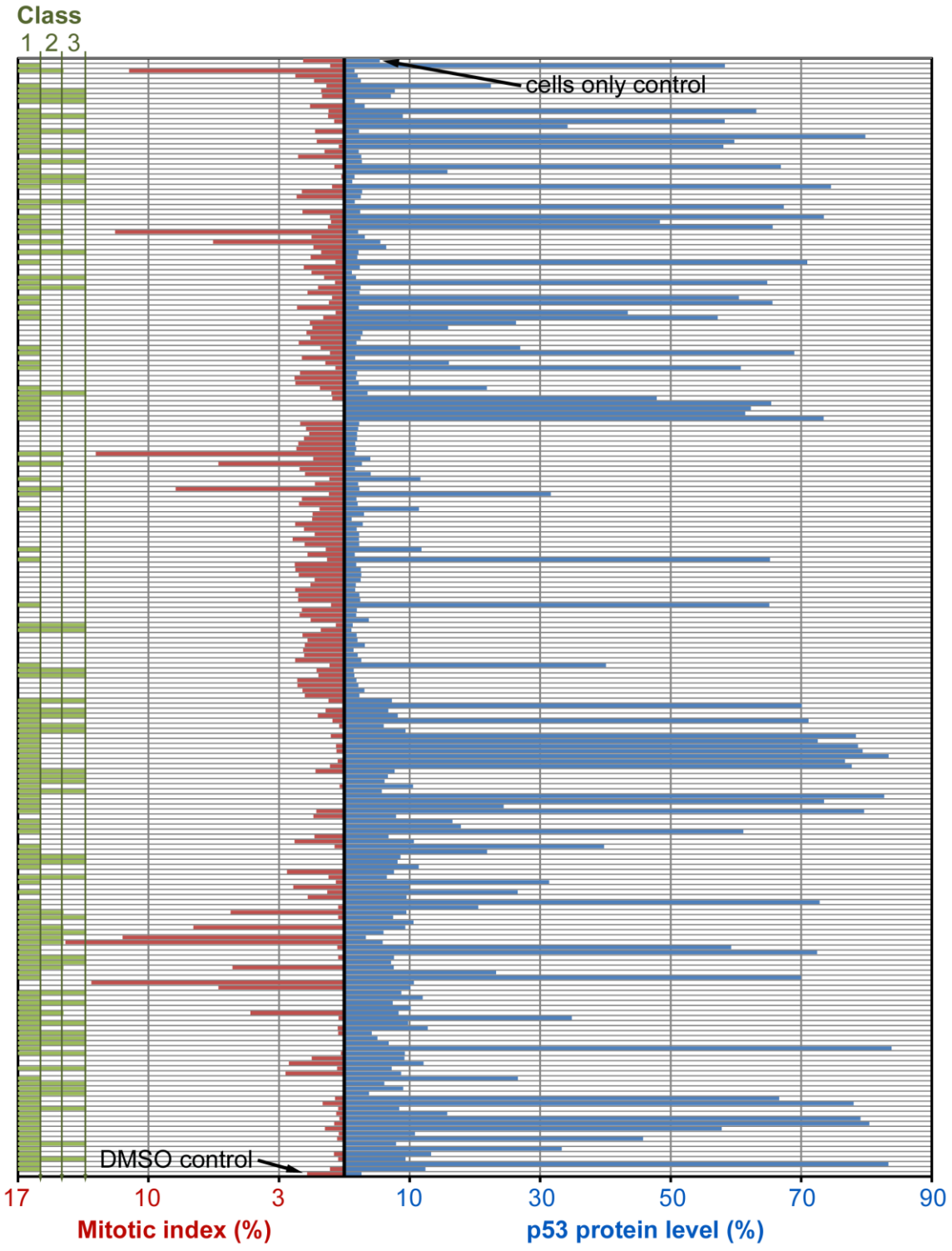

Figure S1 (related to Figure 1). Identification of CDK transcriptional inhibitors by cell-based assays. Cells were treated with a set of 220 test compounds from our 2-anilino-4-(heteroaryl)pyrimidine kinase inhibitor compound library (Wang et al., 2004a; Wang et al., 2004b; Wu et al., 2003) or assay diluent only (DMSO control) at 10 μM for 7 h. MI was measured by determining the percentages of phospho-histone-H3 positive U2-OS cells. Nuclear accumulation of p53 was assessed by immunofluorescent staining in MCF-7 cells. Phenotypic classification is indicated: unclassified; class 1 (transcriptional inhibitors); class 2 (mitotic inhibitors); class 3 (cell cycle inhibitors).

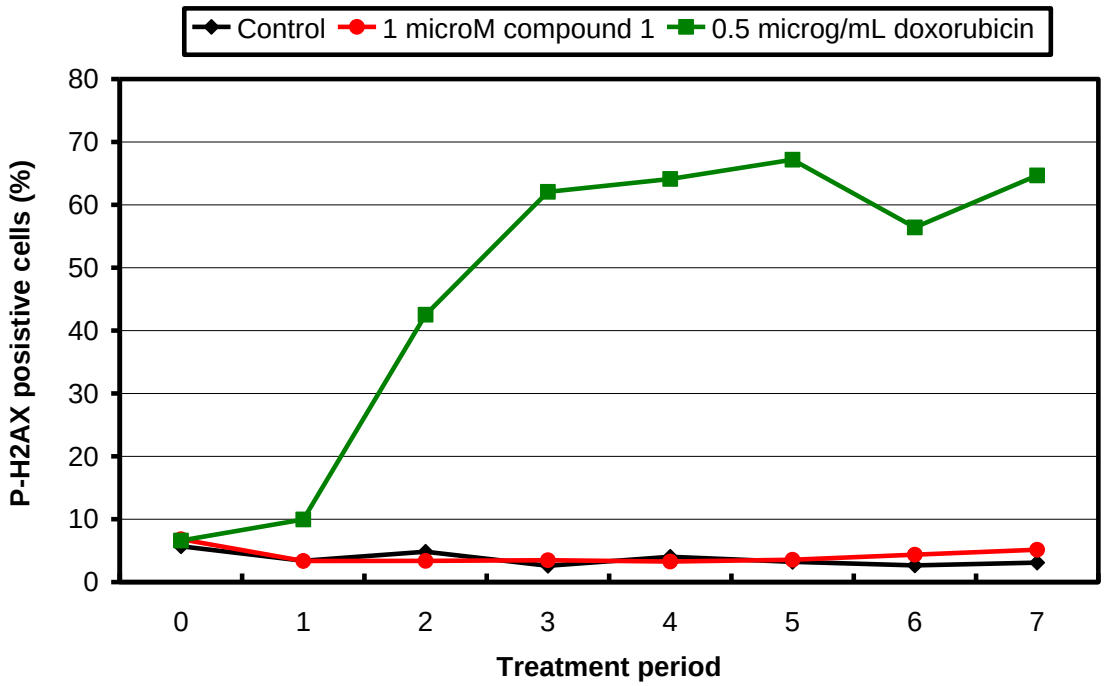

Figure S2 (related to Figure 1). Induction of histone H2AX phosphorylation. Compound **1** does not induce phosphorylation of histone H2AX, (a classical marker of DNA damage) at early time points in contrast to the DNA damaging agent doxorubicin. Cells were treated with compounds or assay diluent only (control) at the concentrations indicated for 7 h.

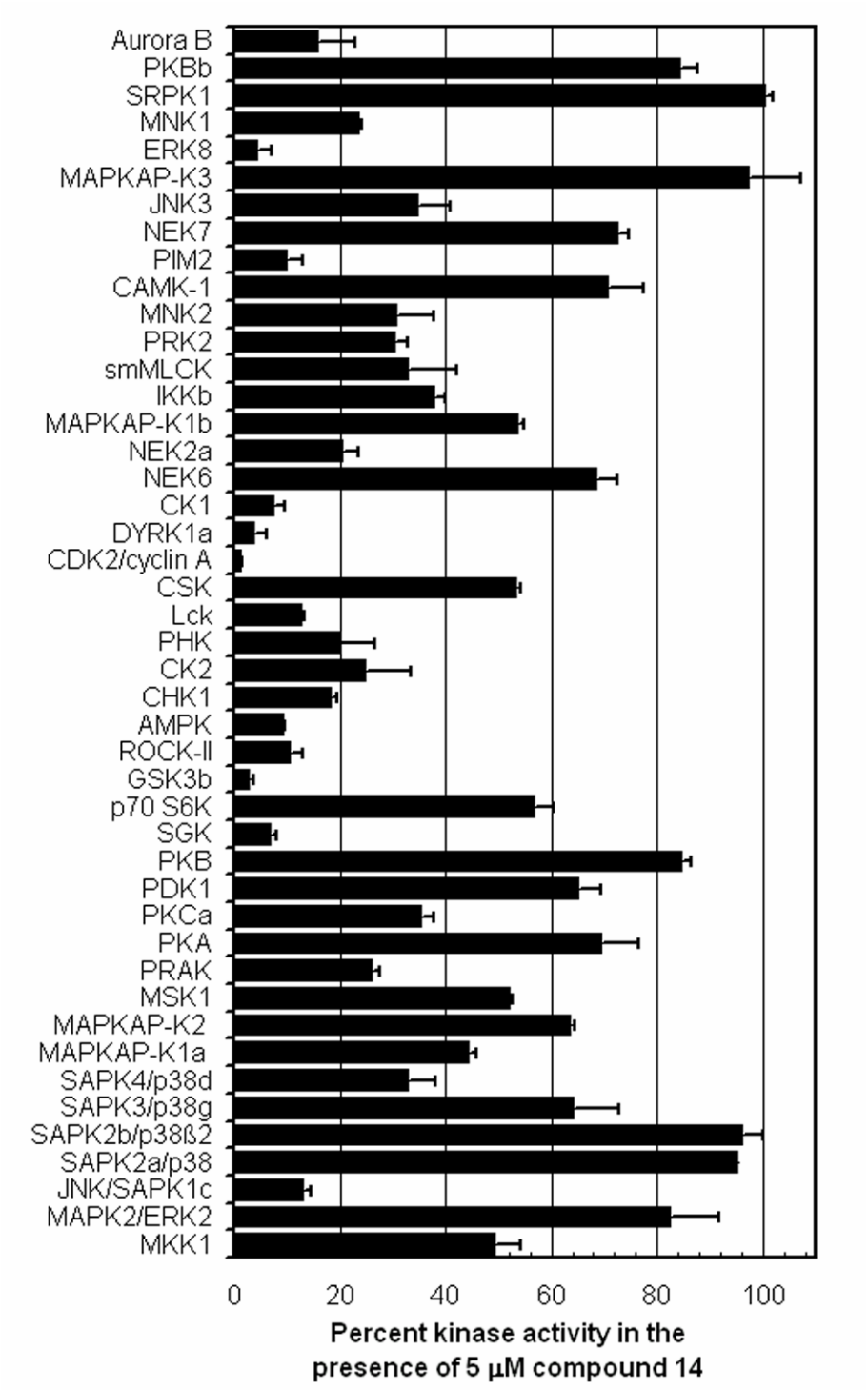

Figure S3 (related to Table 1). Human kinase assay panel for compound 14. The assays were carried out using appropriate protein or peptide substrates and at ATP concentrations near the $K_{m,ATP}$ for the individual kinases (5 – 50 µM).

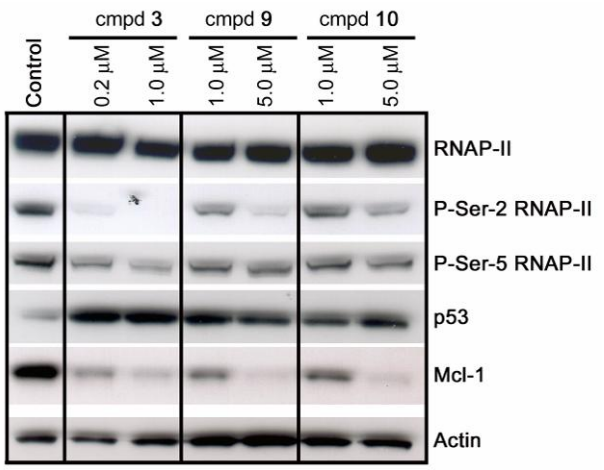

Figure S4 (related to Figure 5). Cellular effects of CDK9-selective compounds. A2780 cells were treated with compounds **3**, **9** and **10** for 3 hours. These compounds represent molecules with a greater selectivity for CDK9 over CDK7 compared to **14**. Each compound can reduce the phosphorylation of RNAP-II CTD at Ser-2, induce p53, and reduce levels of Mcl-1.

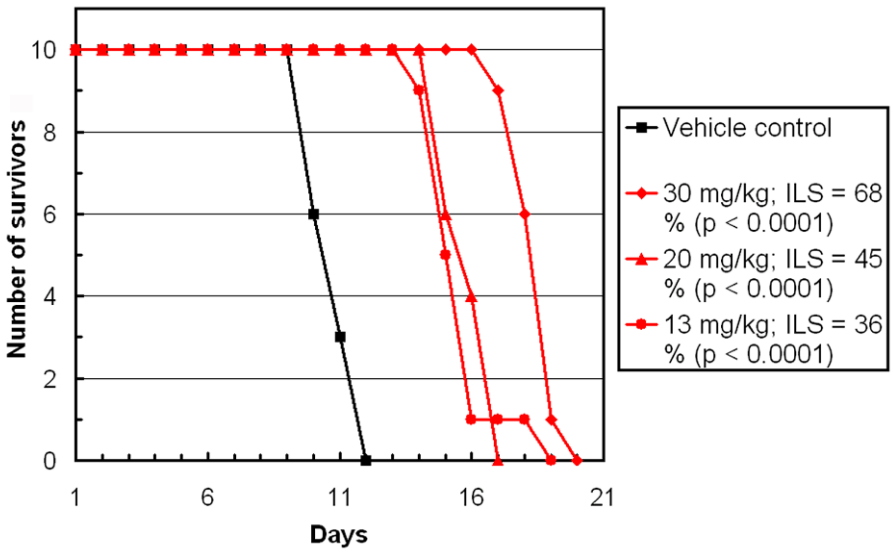

Figure S5 (related to Table 1). *In vivo* antitumour activity of compound 14 in the murine P388/0 survival model. Groups of animals were dosed *ip* with compound **14** twice daily for ten days.

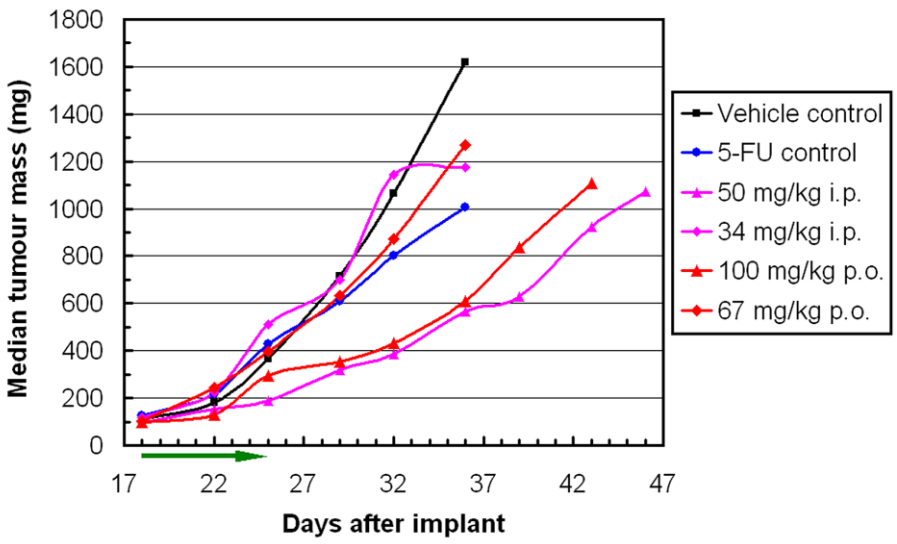

Figure S6 (related to Table 1). ***In vivo*** **antitumour activity of compound 14 in the Colo-205 xenograft model.** Compound **14** was administered once daily for 8 days. The positive control chemotherapy agent 5-FU was given using an optimal dose and schedule for the Colo-205 model. Tumour *versus* control ratios (% T/C) on days 29, 32 and 36: 85, 75 and 62% (5-FU); 45, 36 and 35% (**14**, 50 mg/kg *ip*); 49, 41 and 38% (14, 100 mg/kg *po*). Maximal growth delay (T – C) was 15 days (**14**, 50 mg/kg *ip*) and 12 days (**14**, 100 mg/kg *po*).

Supplemental Experimental Procedures

Synthesis and compound characterisation

3-[4-(2-Ethylamino-4-methyl-thiazol-5-yl)-pyrimidin-2-ylamino]-benzenesulfonamide (**2**). By condensation of 3-dimethylamino-1-(2-ethylamino-4-methyl-thiazol-5-yl)-propenone and nitrate of 3-guanidino-benzenesulfonamide. Yellow solid; mp: 148-150 °C; anal. RP-HPLC (0-60% MeCN): t_R = 13.1 min; ^{1}H-NMR (500 MHz, DMSO-d_6): δ 1.18 (t, J = 7.5 Hz, 3H), 2.48 (s, 3H), 3.27 (m, 2H), 6.94 (d, J = 6.0 Hz, 1H), 7.39 (m, 1H), 7.45 (m, 1H), 7.94 (m, 1H), 8.10 (m, 2H), 8.32 (s, 1H), 8.35 (d, J = 5.5 Hz, 1H), 9.74 (s, 1H); ^{13}C-NMR (125 MHz, DMSO-d_6): δ 14.98, 19.39, 108.13, 116.27, 117.98, 118.89, 122.22, 129.64, 141.78, 145.19, 153.46, 158.25, 159.48, 159.96, 169.45; HRMS (*m/z*): $[M+H]^+$ calcd for $C_{16}H_{19}N_6O_2S_2$, 391.1011; found, 391.1007.

3-[4-(4-Methyl-2-methylamino-thiazol-5-yl)-pyrimidin-2-ylamino]-benzenesulfonamide (**3**). By condensation of 3-dimethylamino-1-(4-methyl-2-methylamino-thiazol-5-yl)-propenone and nitrate of 3-guanidino-benzenesulfonamide. Yellow solid; mp: 276-278 °C; anal. RP-HPLC (0-60% MeCN): t_R = 11.8 min; ^{1}H-NMR (500 MHz, DMSO-d_6): δ 2.73 (s, 3H), 3.12 (d, , J = 5.0 Hz, 3H), 7.20 (d, J = 6.0 Hz, 1H), 7.52 (s, 2H), 7.65 (d, J = 8.0 Hz, 1H), 7.70 (t, J = 8.0 Hz, 1H), 8.18 (d, J = 8.0 Hz, 1H), 8.29 (m, 1H), 8.59 (br s, 1H), 8.61 (d, J = 6.0 Hz, 1H); ^{13}C-NMR (125 MHz, DMSO-d_6): δ 19.8, 31.9, 107.98, 112.50, 116.33, 118.32, 119.01, 122.22, 129.64, 141.77, 145.20, 153.52, 158.28, 159.45, 159.95; HRMS (*m/z*): $[M+H]^+$ calcd for $C_{15}H_{17}N_6O_2S_2$, 377.0854; found, 377.0857.

N-Methyl-3-[4-(4-methyl-2-methylamino-thiazol-5-yl)-pyrimidin-2-ylamino]-benzene-sulfonamide (**4**). By condensation of 3-dimethylamino-1-(4-methyl-2-methylamino-thiazol-5-yl)-propenone and nitrate of 3-guanidino-*N*-methyl-benzenesulfonamide. Yellow solid; mp: 243-245 °C; anal. RP-HPLC (0-60% MeCN): t_R = 13.2 min; ^{1}H-NMR (500 MHz, DMSO-d_6): δ 2.53 (s, 3H), 2.57 (d, J = 5.0 Hz, 3H), 2.99 (s, 3H), 7.00 (d, J = 5.5 Hz, 1H), 7.44 (d, J = 8.0Hz, 1H), 7.48 (t, J = 8.0 Hz, 1H), 7.80 (d, J = 8.0 Hz, 1H), 8.33 (d, J = 5.5 Hz, 1H), 8.52 (s, 1H); ^{13}C-NMR (125 MHz, DMSO-d_6): δ 19.34, 29.46, 31.63, 108.08, 117.12, 118.29, 119.51, 122.66, 129.89, 140.35, 142.01, 153.54, 158.28, 159.40, 159.87, 170.47. HRMS (*m/z*): $[M+H]^+$ calcd for $C_{16}H_{19}N_6O_2S_2$, 391.1011; found, 391.1007.

3-[4-(2-Amino-4-methyl-thiazol-5-yl)-pyrimidin-2-ylamino]-N-methyl-benzenesulfon-amide (**5**). By condensation of 1-(2-amino-4-methyl-thiazol-5-yl)-3-dimethylamino-propenone and nitrate of 3-guanidino-*N*-methyl-benzenesulfonamide. Yellow solid; mp: 206-208 °C; anal. RP-HPLC (0-60% MeCN: t_R = 15.9 min; ^{1}H-NMR (500 MHz, DMSO-d_6): δ 2.43 (s, 3H), 2.44 (s, 3H), 7.14 (d, J = 5.5 Hz, 1H), 7.35 (m, 1H), 7.52 (t, J = 8.0 Hz, 1H), 7.98 (d, J = 8.0 Hz, 1H), 8.30 (s, 1H), 8.58 (d, J = 5.5 Hz, 1H); ^{13}C-NMR (125 MHz, DMSO-d_6): δ 18.54, 19.65, 29.43, 109.85, 117.40, 119.91, 122.89, 130.02, 131.14, 140.40, 141.65, 152.98, 158.74, 160.07, 167.22; HRMS (*m/z*): $[M]^+$ calcd for $C_{15}H_{16}N_6O_2S_2$, 376.0776; found, 376.0774.

(3-Methanesulfonyl-phenyl)-[4-(4-methyl-2-methylamino-thiazol-5-yl)-pyrimidin-2-yl]-amine (**6**). By condensation of 3-dimethylamino-1-(4-methyl-2-methylamino-thiazol-5-yl)-propenone and *N*-(3-methanesulfonyl-phenyl)-guanidine nitrate. Light yellow solid; mp: 272-274 °C; anal. RP-HPLC (0-60% MeCN): t_R = 13.8 min; ^{1}H-NMR (500 MHz, DMSO-d_6): δ 2.86 (s, 3H), 2.87 (s, 3H), 3.20 (s, 3H), 6.98 (d, J = 5.5 Hz, 1H), 7.46 (d, J = 7.5 Hz, 1H), 7.54 (t, J = 7.5 Hz, 1H), 7.95 (m, 1H), 8.08 (m, 1H), 8.38 (d, J = 5.0 Hz, 1H), 8.54 (s, 1H), 9.87 (s, 1H); ^{13}C-NMR (125 MHz, DMSO-d_6): **δ** 19.33, 31.69, 44.47, 108.11, 116.72, 118.29, 119.77, 123.78, 130.15, 141.87, 142.24, 153.64, 158.37, 159.29, 159.78, 161.53; HRMS (*m/z*): $[M+H]^+$ calcd for $C_{16}H_{18}N_5O_2S_2$, 376.0902; found, 376.0902.

[4-(2-Ethylamino-4-methyl-thiazol-5-yl)-pyrimidin-2-yl]-(3-methanesulfonyl-phenyl)-amine (**7**). By condensation of 3-dimethylamino-1-(2-ethylamino-4-methyl-thiazol-5-yl)-

propenone and *N*-(3-methanesulfonyl-phenyl)-guanidine nitrate. Light yellow solid; mp: 220-221 °C; anal. RP-HPLC (0-60% MeCN): t_R = 14.6 min; ^{1}H-NMR (500 MHz, DMSO-d_6): δ 1.19 (t, J = 7.0 Hz, 3H), 2.48 (s, 3H), 2.63-3.17 (m, 5H), 6.97 (d, J = 5.5 Hz, 1H), 7.47 (d, J = 7.5 Hz, 1H), 7.52 (t, J = 7.5 Hz, 1H), 7.94 (m, 1H), 8.16 (m, 1H), 8.38 (d, J = 5.0 Hz, 1H), 8.51 (s, 1H), 9.86 (s, 1H); ^{13}C-NMR (125 MHz, DMSO-d_6): δ 14.93, 19.36, 44.48, 46.00, 108.19, 116.74, 117.94, 119.78, 123.80, 130.17, 141.87, 142.27, 153.60, 158.34, 159.35, 159.80, 169.51; HRMS (*m/z*): $[M+H]^+$ calcd for $C_{17}H_{20}N_5O_2S_2$, 390.1058; found, 390.1060.

3-[4-(2-Amino-4-methyl-thiazol-5-yl)-pyrimidin-2-ylamino]-N-ethyl-benzenesulfonamide (**8**). By condensation of 1-(2-amino-4-methyl-thiazol-5-yl)-3-dimethylamino-propenone and nitrate of *N*-ethyl-3-guanidino-benzenesulfonamide. Yellow solid; mp: 176-177 °C; anal. RP-HPLC (0-60 % MeCN%): t_R = 13.5 min; ^{1}H-NMR (500 MHz, DMSO-d_6): δ 1.08 (t, J = 7.5 Hz, 3H), 2.51 (s, 3H), 2.95 (m, 2H), 6.98 (d, J = 5.5 Hz, 1H), 7.44-7.49 (m, 2H), 7.89 (d, J = 7.5 Hz, 1H), 8.34 (d, J = 5.5 Hz, 1H), 8.37 (br s, 1H); HRMS (*m/z*): $[M+H]^+$ calcd for $C_{16}H_{19}N_6O_2S_2$, 391.1011; found, 391.1007.

[4-(4-Methyl-2-methylamino-thiazol-5-yl)-pyrimidin-2-yl]-[4-methyl-3-(morpholine-4-sulfonyl)-phenyl]-amine (**9**). By condensation of 3-dimethylamino-1-(4-methyl-2-methylamino-thiazol-5-yl)-propenone and *N*-[4-methyl-3-(morpholine-4-sulfonyl)-phenyl]-guanidine nitrate. Light yellow solid; mp: 237-238 °C; anal. RP-HPLC (0-60% MeCN): t_R = 15.8 min; ^{1}H-NMR (500 MHz, DMSO-d_6): δ 2.53 (s, 3H), 2.59 (s, 3H), 2.99 (s, 3H), 3.16 (m, 4H), 3.70 (m, 4H), 6.97 (d, J = 5.5 Hz, 1H), 7.34 (d, J = 8.0 Hz, 1H), 7.80 (d, J = 8.0 Hz, 1H), 8.31 (d, J = 5.0 Hz, 1H), 8.41 (s, 1H); ^{13}C-NMR (125 MHz, DMSO-d_6): δ 19.38, 20.38, 31.61, 46.03, 66.30, 108.02, 118.29, 119.89, 123.51, 129.75, 133.71, 135.34, 139.74, 153.47, 158.27, 159.50, 159.94, 170.38. HRMS (*m/z*): $[M+H]^+$ calcd for $C_{20}H_{25}N_6O_3S_2$, 461.1430; found, 461.1433.

[4-(2-Amino-4-methyl-thiazol-5-yl)-pyrimidin-2-yl]-[4-methyl-3-(morpholine-4-sulfonyl)-phenyl]-amine (**10**). By condensation of 1-(2-amino-4-methyl-thiazol-5-yl)-3-dimethylamino-propenone and *N*-[4-methyl-3-(morpholine-4-sulfonyl)-phenyl]-guanidine nitrate. Light yellow solid; mp: 183-184 °C; anal. RP-HPLC (0-60% MeCN): t_R = 15.5 min. ^{1}H-NMR (500 MHz, DMSO-d_6): δ 2.76 (s, 3H), 2.82 (s, 3H), 3.38 (m, 4H), 3.95 (m, 4H), 7.23 (d, J = 5.5 Hz, 1H), 7.66 (d, J = 9.0 Hz, 1H), 7.83 (s, 2H), 8.41 (m, 1H), 8.66 (d, J = 5.0 Hz, 1H); ^{13}C-NMR (125 MHz, DMSO-d_6): δ 19.16, 20.33, 46.03, 66.32, 108.31, 118.33, 120.11, 123.47, 129.70, 133.66, 135.41, 139.72, 153.12, 158.24, 159.63, 159.95, 169.62. HRMS (*m/z*): $[M+H]^+$ calcd for $C_{19}H_{23}N_6O_3S_2$, 447.1273; found 447.1271.

4-[4-(3,4-Dimethyl-2-oxo-2,3-dihydro-thiazol-5-yl)-pyrimidin-2-ylamino]-N-(2-methoxy-ethyl)-benzenesulfonamide (**11**). By condensation of 5-(3-dimethylamino-acryloyl)-3,4-dimethyl-3*H*-thiazol-2-one and nitrate of 4-guanidino-*N*-(2-methoxy-ethyl)-benzenesulfonamide; Yellow solid; mp: 238-239 °C; anal. RP-HPLC (0-60% MeCN): t_R = 16.3 min; ^{1}H-NMR (500 MHz, DMSO-d_6): δ 2.52 (s, 3H), 2.82 (q, J = 6.0, 12.0 Hz, 2H), 3.10 (s, 3H), 3.23 (m, 2H), 3.25 (s, CH_3), 7.00 (d, J = 5.5 Hz, 1H), 7.43 (t, J = 6.0 Hz, 1H), 7.64 (d, J = 9.0 Hz, 2H), 7.87 (d, J = 9.0 Hz, 2H), 8.44 (d, J = 5.5 Hz, 1H); ^{13}C-NMR (125 MHz, DMSO-d_6): δ 15.02, 30.35, 42.83, 58.56, 71.25, 110.08, 110.24, 118.85, 128.12, 133.08, 139.03, 144.63, 158.61, 159.30, 159.77, 170.37; HRMS (*m/z*): $[M+H]^+$ calcd for $C_{18}H_{22}N_5O_4S_2$, 436.1113; found 436.1111.

3-[4-(3,4-Dimethyl-2-oxo-2,3-dihydro-thiazol-5-yl)-pyrimidin-2-ylamino]-benzonitrile (**12**). By treatment of 5-(3-dimethylamino-acryloyl)-3,4-dimethyl-3*H*-thiazol-2-one and *N*-(3-cyano-phenyl)-guanidine nitrate; anal. RP-HPLC (10-70% MeCN): t_R = 15.5 min; ^{1}H-NMR (500 MHz, DMSO-d_6): δ 2.52 (s, 3H), 3.29 (s, 3H), 7.06 (d, J = 5.5 Hz, 1H), 7.40 (m, 1H), 7.51 (t, J = 8.0 Hz, 1H), 7.93 (m, 1H), 8.33 (s, 1H), 8.50 (d, J = 5.5 Hz, 1H), 10.00 (s, 1H); ^{13}C-NMR (125 MHz, DMSO-d_6): δ 14.97, 30.32, 109.94, 109.95, 112.05, 119.76, 121.89, 124.04, 125.43, 130.61, 139.02, 141.91, 158.55, 159.34, 159.78, 170.36; HRMS (*m/z*): $[M+H]^+$ calcd for $C_{16}H_{14}N_5OS$, 324.0919; found 324.0927.

3,4-Dimethyl-5-[2-(4-methyl-3-nitro-phenylamino)-pyrimidin-4-yl]-3H-thiazol-2-one (**13**). By condensation of 5-(3-dimethylamino-acryloyl)-3,4-dimethyl-3*H*-thiazol-2-one and *N*-(3-cyano-4-methyl-phenyl)-guanidine nitrate; anal. RP-HPLC (10-70% MeCN): t_R = 17.6 min; ^{1}H-NMR (500 MHz, DMSO-d_6): δ 2.44 (s, 3H), 2.55 (s, 3H), 3.28 (s, 3H), 7.03 (d, J = 5.5 Hz, 1H), 7.40 (d, J = 9.0 Hz, 1H), 7.84 (d, J = 9.0 Hz, 1H), 8.48 (d, J = 5.5 Hz, 1H,), 8.59 (s, 1H), 9.99 (s, 1H); ^{13}C-NMR (125 MHz, DMSO-d_6): δ 14.96, 19.70, 30.32, 109.79, 114.22, 124.13, 125.63, 133.42, 138.94, 140.07, 149.44, 158.54, 159.33, 159.80, 170.41; HRMS (*m/z*): $[M+H]^+$ calcd for $C_{16}H_{16}N_5O_3S$, 358.0974; found, 358.0976.

3,4-Dimethyl-5-[2-(4-piperazin-1-yl-phenylamino)-pyrimidin-4-yl]-3H-thiazol-2-one (**14**). A solution of potassium thiocyanate (5.67 g, 58 mmol) in Me_2CO (45 mL) was cooled on ice and 3-chloro-pentane-2,4-dione (6.95 mL, 58 mmol) was added dropwise. The mixture was warmed to room temperature and stirred for 6 h. After evaporation to dryness, the residue was dissolved in EtOH (30 mL) and conc. aq HCl (15 mL) was added. This mixture was heated to reflux for 14 h. After cooling, it was concentrated and the resulting precipitates were filtered and washed successively with cold MeOH and Et_2O to afford 5-acetyl-4-methyl-3*H*-thiazol-2-one (9.1 g, 100%). mp 208-211 °C; anal. RP-HPLC (10-70% MeCN): t_R = 6.5 min; ^{1}H-NMR (500 MHz, $CDCl_3$): δ 2.33 (s, 3H), 2.38 (s, 3H), 11.9 (s, 1H); ^{13}C-NMR (125 MHz, DMSO-d_6): δ 15.06, 29.94, 115.53, 142.99, 170.92, 189.91; FTIR: 3094, 2850, 1669, 1622, 1579 cm^{-1}; MS (*m/z*): $[M+H]^+$ calcd for $C_6H_8NO_2S$, 158.19; found 157.77.

5-Acetyl-4-methyl-3*H*-thiazol-2-one (4.64 g, 27.1 mmol) and *N*,*N*-dimethylformamide dimethylacetal (8.4 mL, 59.6 mmol) were mixed in a dry, Ar-flushed flask, and the mixture was heated at 100 °C for 3 h. After cooling, an equal volume of Et_2O was added. The resulting orange solid was filtered and washed with Et_2O to afford 2.73 g of 5-(3-dimethylamino-acryloyl)-3,4-dimethyl-3*H*-thiazol-2-one as an orange solid. ^{1}H-NMR (500 MHz, DMSO-d_6): δ 2.52 (s, 3H), 2.82 (br s, 3H), 3.11 (br s, 3H), 3.22 (s, 3H), 5.10 (d, J = 12.2Hz, 1H,), 7.61 (d, J = 11.7 Hz, 1H).

N-[4-(4-Acetyl-piperazin-1-yl)-phenyl]-guanidine nitrate was prepared following the procedures described previously (Wang et al., 2004a). The reaction mixture was filtered through Celite and concentrated under reduced pressure. Recrystallisation from EtOH gave the pure product as a pale pink solid (91%). ^{1}H-NMR (500 MHz, DMSO-d_6): δ 2.06 (s, 3H), 3.15 (m, 4H), 3.58 (m, 4H), 7.04-7.19 (m, 8H), 9.32 (s, 1H).

A solution of 5-(3-dimethylamino-acryloyl)-3,4-dimethyl-3*H*-thiazol-2-one (0.20 g, 0.88 mmol), *N*-[4-(4-acetyl-piperazin-1-yl)-phenyl]-guanidine nitrate (0.38 g, 1.15 mmol) and NaOH (0.09 g, 2.3 mmol) in 2-methoxylethanol (15 mL) was heated at 120 °C for 20 h. The reaction mixture was evaporated to dryness and the residue was purified by silica gel chromatography, eluting with CH_2Cl_2, then 2% MeOH/CH_2Cl_2 to afford 5-[2-[4-(4-acetyl-piperazin-1-yl)-phenylamino]-pyrimidin-4-yl]-3,4-dimethyl-3*H*-thiazol-2-one as a yellow solid (0.22 g, 60 %). Mp. 231-234 °C; anal. RP-HPLC (10-70% MeCN): t_R = 9.5 min; ^{1}H-NMR (500 MHz, DMSO-d_6): δ 2.03 (s, 3H), 2.55 (s, 3H), 3.01 (m, 2H), 3.08 (m, 2H), 3.29 (s, 3H), 3.57 (m, 4H), 6.87 (d, J = 5.5 Hz, 1H), 6.93 (d, J = 9.0 Hz, 2H), 7.58 (d, J = 9.0 Hz, 2H), 8.37 (d, J = 5.5 Hz, 1H), 9.37 (s, 1H); Analysis (calcd, found for $C_{21}H_{24}N_6O_2S$): C (58.41, 58.49), H (5.70, 5.77), N (19.80, 19.33).

This material, in 2 M HCl in EtOH, was heated under reflux for 2.5 h. After cooling, the mixture was evaporated, the residue was basified by addition of 2 M aq NaOH and extracted (2 × 50 mL CH_2Cl_2). The combined extracts were washed with brine, dried on $MgSO_4$, and filtered. The solvent was evaporated and the residue was crystallised from MeOH to afford 3,4-dimethyl-5-[2-(4-piperazin-1-yl-phenylamino)-pyrimidin-4-yl]-3*H*-thiazol-2-one (**14**) as a yellow solid (90%). mp. 224-226 °C; anal. RP-HPLC (0-60% MeCN): t_R = 10.9 min; ^{1}H-NMR (500 MHz, DMSO-d_6): δ 2.57 (s, 3H), 3.10 (m, 4H), 3.16 (m, 4H), 3.36 (s, 3H), 6.65 (d, J = 5.5 Hz, 1H), 6.94 (d, J = 10.5 Hz, 2H), 7.47 (d, J = 9.0 Hz, 2H), 8.31 (d, J = 5.5 Hz, 1H); ^{13}C-NMR (125 MHz, DMSO-d_6): δ 14.85, 30.20, 46.35, 50.84, 108.18, 110.62, 116.36, 121.11, 132.83, 138.18, 147.69, 158.38, 159.13,

160.33, 170.42. Analysis (calcd, found for $C_{19}H_{22}N_6OS \cdot 0.45\ H_2O$): C (59.55, 59.32), H (6.10, 6.14), N (25.59, 24.97).

Cloning, expression, and purification of His-tagged CDK9/Cyclin T1

Cloning and expression of His-tagged CDK9/cyclin T1. Baculoviral transfer vector pFastBac HTa (Invitrogen, Carlsbad, USA) was modified to produce pSSP1, by replacing the region between the *Rsr* II and *Eco* RI restriction endonuclease sites of pFastBac HTa with a double stranded linker corresponding to sense strand 5'-GTCCGTCCGAAACCAT GTCGTACTACCATCACCATCACCATCACGGTATGGCTAGCGACGATGACGATAAGGGATCCGTGC GGCCGCG-3'. This modification was introduced to allow expression of fusion proteins where the N-terminal polyhistidine tag (His-tag) could be removed by cleavage at an enterokinase cleavage site introduced immediately adjacent to the polypeptide encoded by the inserted gene of interest.

The CDK9 open reading frame was amplified from a human foetal lung 5'-Stretch Plus cDNA library (Clontech, Palo Alto, USA) using PCR primer 1 (5'-GCGTTGGAGGCGGCCATG GCAAAGCAGTACG-3') and 2 (5'-CTAGTGGCAAGCGCCGGCCCTCAGAAG-3'). The amplified DNA fragment was cloned into pCR4-Topo (Invitrogen, Carlsbad, USA), to give pCR4-CDK9. PCR primer 3 (5'-GGCGCTAGCGACGATGACGATAAGATGGCAAAGCAGTACGACTCG-3') and 4 (5'-CAGGAAACAGCTATGAC-3') were used to amplify the CDK9 open reading frame from pCR4-CDK9. The PCR product generated was digested with *Nhe* I and *Eco* RI and ligated into pSSP1, also digested with *Nhe* I and *Eco* RI. Insert DNA from several clones was sequenced, and fragment exchange was used to generate a single clone, pSSP1-Cdk9 with the correct CDK9 coding sequence.

The cyclin T1 open reading frame was amplified as two fragments from a human foetal lung 5'-Stretch Plus cDNA library (Clontech, Palo Alto, USA), using PCR primer 5 (5'-ATGGAGGGAGAGAGGAAGAACAACAACAAACGGTGGTAT-3') and 6 (5'-GTAAGTGCTAAATTC TCACTAGTCCG-3'), or PCR primer 7 (5'-CTACTCAGGG TCATCGGACT AGTGAG-3') and 8 (5'-TTACTTAGGAAGGGGTGGAAGTGGTGGAGGAGGTTCTGA-3'). Each of the PCR products generated were cloned into pCR4-Topo, giving pCR4-5'Cyclin T1 and pCR4-3'cyclin T1, respectively. The sequence of these PCR fragments was confirmed. The cyclin T1 fragment of pCR4-5'cyclin T1 was then amplified using PCR primer 9 (5'-GGCGCTAGCGACGATGACGATAAGATGGAGGGAGAGAGGAAGAACAAC-3') and 4 (5-CAGGA AACAGCTATGAC-3'), to introduce an *Nhe* I restriction endonuclease site upstream of the Cyclin T1 coding sequence. The resulting PCR product was digested with *Nhe* I and *Eco* RI and then ligated into pSSP1, also digested with *Nhe* I and *Eco* RI, to give pSSP-5'cyclin T1. The complete cyclin T1 open reading frame was subsequently generated by digesting pCR4-3'cyclin T1 with *Not* I and *Spe* I, and ligating the required fragment into pSSP-5'cyclin T1, also digested with *Not* I and *Spe* I, to create pSSP1-cyclin T1.

Bacmid DNA and baculoviral stocks were generated from pSSP1-CDK9 and pSSP1-cyclin T1 according to the manufacturer's instructions for pFastBac HTa. High-titre baculoviral stocks were generated by amplification in Sf9 cells grown in suspension culture. Viral titres were determined by standard plaque assay protocols, as per the manufacturer's instructions.

His-tagged CDK9 and cyclin T1 were co-expressed following co-infection of Sf9 cells by SSP1-CDK9 and SSP1-cyclin T1 baculoviruses. 72 h post-infection, cells were harvested by centrifugation, and snap frozen. Recombinant protein expression levels were confirmed by western blotting, using CDK9 sc-8338 and cyclinT1 sc-10750 antibodies (Santa Cruz Biotechnology, Inc., Santa Cruz, USA).

Protein Purification. The Sf9 cell pellet from 300 mL cell culture was lysed in 30 mL of 25 mM HEPES pH 7.5, 0.02 mM EGTA, 0.02 mM EDTA, 270 mM sucrose, 1% Triton X-100, 0.07% β-mercaptoethanol, 1 mM Na_3VO_4, 5 mM NaF, 0.2 mM PMSF, 1 mM benzamidine, protease inhibitor cocktail (Sigma, St. Louis, USA). After incubating on ice for 20 min, the samples were cleared by centrifuging for 20 min at 15,000 rpm. The result-

ing supernatant was supplemented with NaCl to 0.3 M, and then 1.2 mL (pre-equilibrated) Ni-NTA beads were added. After 1.5 h constant rotation at 4 °C, samples were centrifuged for 2 min at 2,000 rpm and supernatant was removed. Beads were re-suspended in 10 mL of 25 mM HEPES pH 7.5, 0.02 mM EGTA, 0.02 mM EDTA, 0.5 M NaCl, 20 mM imidazole, 0.03% Brij-35, 0.07% β-mercaptoethanol, 0.2 mM PMSF, 1 mM benzamidine then and transferred to a 12 mL column. Washing was performed twice with 10 mL of 25 mM HEPES pH 7.5, 0.02 mM EGTA, 0.02 mM EDTA, 0.5 M NaCl, 20 mM imidazole, 0.03% Brij-35, 0.07% β-mercaptoethanol, 0.2 mM PMSF, 1 mM benzamidine, and then twice with 10 mL of 25 mM HEPES pH 7.5, 0.02 mM EGTA, 0.02 mM EDTA, 0.3 M NaCl, 0.03% Brij-35, 0.07% β-mercaptoethanol, 0.2 mM PMSF, 1 mM benzamidine. CDK9/cyclin T1 was eluted with three washes of 2 mL of 25 mM HEPES pH 7.5, 0.02 mM EGTA, 0.02 mM EDTA, 0.3 M NaCl, 0.03% Brij-35, 0.07% β-mercaptoethanol, 0.2 mM PMSF, 1 mM benzamidine, 200 mM imidazole. CDK9/cyclin T1-containing fractions were identified by Western blotting. These fractions were combined and then dialysed overnight against 100 volumes of 50 mM Tris/HCl pH7.5, 0.1 mM EGTA, 150 mM NaCl, 270 mM sucrose, 0.03% Brij-35, 0.07% β-mercaptoethanol, 1 mM benzamidine, 0.1 mM PMSF. Protein concentration was determined by BCA assay. Samples were snap frozen in 100 µL aliquots, and stored at -70 °C. Specific activity was determined prior to use in screening assays.

Biopharmaceutical profiling and PK determinations

Test compound partitioning between octanol and aqueous buffer was carried out using the shake-flask method (Dearden, 1985). Compound pK_a values were determined using a pH-metric titration method (GlpKa; Sirius) (Comer, 2003). Aqueous solubility was assessed by turbidimetric measurements (Brooker et al., 1974). Apparent permeability coefficients were measured using a Caco-2 cell layer assay (Gan et al., 1997). *In vitro* phase-I liver metabolism was assessed by disappearance of parent compound (LC-MS quantitation) from a preparation of rat liver microsomes (Houston et al., 1997). Rat plasma protein binding was determined in an equilibrium dialysis assay (Kariv et al., 2001).

For PK measurements 3 male Wistar rats per sample and dose were treated by *iv* bolus injection or by *po* gavage of test compound solutions. Blood samples were collected from each rat from the cannulated jugular vein at time zero and at intervals up to 24 h. Samples were centrifuged immediately and plasma was harvested and frozen at –20 °C until analysis. Quantitative compound level analysis was carried out using LC-MS/MS methods. PK parameters were derived by the noncompartmental methods using the WinNonlin 3.2 software programme (Pharsight). Oral bioavailability (%F) was calculated by taking the ratio of dose-normalised AUC values from oral *versus* parenteral dosing.

Evaluation of anti-tumour efficacy

Murine P388/0 leukaemia model. Six-week-old male CD2F1 mice were implanted intraperitoneally with P388/0 leukaemia cells (10^5) on day 0. On day 1 post-inoculation mice were given by *ip* administration either vehicle or test compound (0.1 mL / 10 g body weight) at the dose shown, on a treatment schedule of twice a day for 10 days. The effectiveness of treatment was assessed by comparison of the median post-inoculation lifespan (ILS) of each group of treated mice with that of the vehicle control group. The ILS ratio of the treated and control groups was used as an indicator of efficacy.

Colo-205 xenograft model. Female athymic ICR SCID mice, 5-6 weeks old on day 1 of the treatment, were used for this study. Test animal were implanted subcutaneously on day 0 with 30-60 mg tumour fragments using a 12-gauge trocar needle. Treatment began on day 18 when the mean estimated tumour mass for all groups in the study was 107 mg (range 97-115 mg). The animals were assigned into the treatment and the control groups with 10 mice per group. All animals were observed for clinical signs at least once daily. Tumour size was measured at least twice weekly. Animals were terminated at any time during the study if the tumour size became excessive or any adverse effects

were noted. The treatments were administered by *ip* injection or *po* gavage daily, staring on day 18, and continuing for 8 days. The tumour burden (mg) was estimated from calliper measurements using the formula for the volume of a prolate ellipsoid assuming unit density. The mean tumour mass on the day of randomisation was reported for each group. Calculations of relative tumour mass and plot of mean tumour growth curves were performed. The relative tumour mass data from each group were compared using a one-way analysis of variance (ANOVA) and statistical significance was determined using the built-in data analysis tools in Microsoft Excel and R (The R Project for Statistical Computing).

Crystallography

Human recombinant CDK2 was expressed, purified, and crystallised as previously described (Wu et al., 2003). Data were collected at the Cyclacel home source with a FR-D X-ray generator using a Raxis IV++ image plate (Rigaku). Data processing was carried out using the d*TREK software suite (Pflugrath, 1999). The structures were solved by molecular replacement using MOLREP (Vagin et al., 1997) and PDB entry 1PW2. ARP/wARP (Lamzin et al., 1997) was used for initial density interpretation and the addition of water molecules. REFMAC (Murshudov et al., 1997) was used for structural refinement. A number of rounds of refinement and model building with the programme COOT (Emsley et al., 2010) were carried out. All the crystallographic programmes used were part of the *CCP4* programme suite (Potterton et al., 2004).

Supplemental References

Brooker, P.J., and Ellison, M. (1974). Determination of the water solubility of organic compounds by a rapid turbidimetric method. Chem. Ind., 285-287.

Comer, J.E.A. (2003). High-throughput measurement of log D and pKa. Methods Principles Med. Chem. *18*, 21-45.

Dearden, J.C. (1985). Partitioning and lipophilicity in quantitative structure-activity relationships. Environ. Health Persp. *61*, 203-228.

Gan, L.-S.L., and Thakker, D.R. (1997). Applications of the Caco-2 model in the design and development of orally active drugs: elucidation of biochemical and physical barriers posed by the intestinal epithelium. Adv. Drug Delivery Rev. *23*, 77-98.

Houston, J.B., and Carlile, D.J. (1997). Prediction of hepatic clearance from microsomes, hepatocytes, and liver slices. Drug Metabol. Rev. *29*, 891-922.

Kariv, I., Cao, H., and Oldenburg, K.R. (2001). Development of a high throughput equilibrium dialysis method. J. Pharm. Sci. *90*, 580-587.

Lamzin, V.S., and Wilson, K.S. (1997). Automated refinement for protein crystallography. Methods Enzymol. *277*, 269-305.

Murshudov, G.N., Vagin, A.A., and Dodson, E.J. (1997). Refinement of macromolecular structures by the maximum-likelihood method. Acta Crystallogr. *D53*, 240-255.

Pflugrath, J.W. (1999). The finer things in X-ray diffraction data collection. Acta Crystallogr. *D55* 1718-1725.

Potterton, L., McNicholas, S., Krissinel, E., Gruber, J., Cowtan, K., Emsley, P., Murshudov, G.N., Cohen, S., Perrakis, A., and Noble, M. (2004). Developments in the CCP4 molecular-graphics project. Acta Crystallogr. *D60*, 2288-2294.

Vagin, A., and Teplyakov, A. (1997). MOLREP: an automated program for molecular replacement. J. Appl. Crystallogr. *30*, 1022 -1025.

Wang, S., Meades, C., Wood, G., Osnowski, A., Anderson, S., Yuill, R., Thomas, M., Mezna, M., Jackson, W., Midgley, C., Griffiths, G., Fleming, I., Green, S., McNae, I., Wu, S.-Y., McInnes, C., Zheleva, D., Walkinshaw, M.D., and Fischer, P.M. (2004a). 2-Anilino-4-(thiazol-5-yl)pyrimidine CDK Inhibitors: Synthesis, SAR analysis, X-Ray Crystallography, and Biological Activity. J. Med. Chem. *47*, 1662-1675.

Wang, S., Wood, G., Meades, C., Griffiths, G., Midgley, C., McNae, I., McInnes, C., Anderson, S., Jackson, W., Mezna, M., Yuill, R., Walkinshaw, M., and Fischer, P.M. (2004b). Synthesis and Biological Activity of 2-Anilino-4-(1H-pyrrol-3-yl)pyrimidine CDK Inhibitors. Bioorg. Med. Chem. Lett. *14*, 4237-4240.

Wu, S.Y., McNae, I., Kontopidis, G., McClue, S.J., McInnes, C., Stewart, K.J., Wang, S., Zheleva, D.I., Marriage, H., Lane, D.P., Taylor, P., Fischer, P.M., and Walkinshaw, M.D. (2003). Discovery of a Novel Family of CDK Inhibitors with the Program LIDAEUS: Structural Basis for Ligand-Induced Disordering of the Activation Loop. Structure *11*, 399-410.